

From Answers to Rationales: Self-Aligning Multimodal Reasoning with Answer-Oriented Chain-of-Thought

Wentao Tan^{1,2} Qiong Cao^{2†*} Yibing Zhan^{2†} Chao Xue² Changxing Ding^{1,3}
¹South China University of Technology ²JD Explore Academy, Beijing ³Pazhou Lab, Guangzhou
 ftwentaotan@mail.scut.edu.cn, caoqiong1@jd.com, zybji@mail.ustc.edu.cn
 xuechao19@jd.com, chxding@scut.edu.cn

Abstract

Achieving human-like reasoning capabilities in Multimodal Large Language Models (MLLMs) has long been a goal. Current methodologies primarily focus on synthesizing positive rationales, while overlooking the critical role of negative rationales in training models to discern flawed reasoning patterns. To address this gap, we propose a novel framework: Self-Aligning Multimodal Reasoning with Answer-Oriented Chain-of-Thought (SMART). This framework enables models to utilize AoT-Oriented Chain-of-Thought (AoT) prompts to automatically generate high-quality positive and negative reasoning paths, followed by self-alignment to enhance their reasoning abilities. Inspired by human strategies for solving proof-based problems, AoT uses answers as a guide to help the model extract critical visual information that links questions and answers. When provided with ground truth answers, the model produces strong positive rationales. Conversely, when correct answers are replaced with misleading alternatives, the model generates an erroneous yet compelling reasoning path, serving as a form of discriminative negative rationale. Models trained with AoT-generated data outperform those trained on manually annotated datasets, demonstrating superior reasoning capabilities. This encourages the use of improved models to generate higher-quality preference data for further optimization. Consequently, SMART establishes an iterative generation-optimization method that continually enhances the model’s reasoning skills. Experiments indicate that the SMART framework significantly improves various MLLMs, regardless of model architecture, parameter size, or pre-training dataset. The code, datasets, and models will be released.

1. Introduction

Recently, there has been significant progress in Multimodal Large Language Models (MLLMs) [6, 7, 11, 22, 28, 30, 45, 56]. Many impressive visual-text MLLMs [10, 33, 34, 52, 55, 57] have emerged, demonstrating excellent performance in tasks like image captioning [31, 51] and visual question answering [2, 16, 26]. However, as task complexity increases, these models reveal limitations in their reasoning abilities. For example, while they perform well on simple benchmarks, they struggle with more complex tasks that require logical reasoning [8, 37, 59]. Developing AI systems capable of complex multimodal reasoning, akin to human cognition, is a key objective in the MLLM field. Therefore, enhancing the reasoning capabilities of these models is of utmost importance.

One of the most common approaches involves curating labeled multimodal reasoning datasets for training. Previous works have focused on creating positive rationales for Supervised Fine-Tuning (SFT) datasets, often relying on time-consuming manual annotations [8, 36] (Fig. 1 (a)). Some researchers [17, 40, 63, 64] developed innovative chain-of-thought (CoT) prompts that enable models to generate reasoning datasets without extensive training. These approaches typically require both MLLM and LLM. The LLM first analyzes the problem and generates sub-questions to request the necessary visual details. The MLLM then converts the visual information into text, and finally, the LLM summarizes the results (Fig. 1 (b)). However, this method complicates the system and limits the LLM’s effectiveness due to it can not “see” the images, leading to potential errors. Streamlined alternatives employ a single MLLM to execute the entire CoT process (Fig. 1 (c)). They prompt the MLLM to extract critical visual information, e.g., scene graphs [39] or image descriptions [54], as prior knowledge for answering questions. While efficient, it struggles with tasks like mathematical geometry reasoning, where accurate visual interpretation is difficult [8]. Moreover, the aforementioned methods can only gen-

*Project Lead.

†Corresponding Authors.

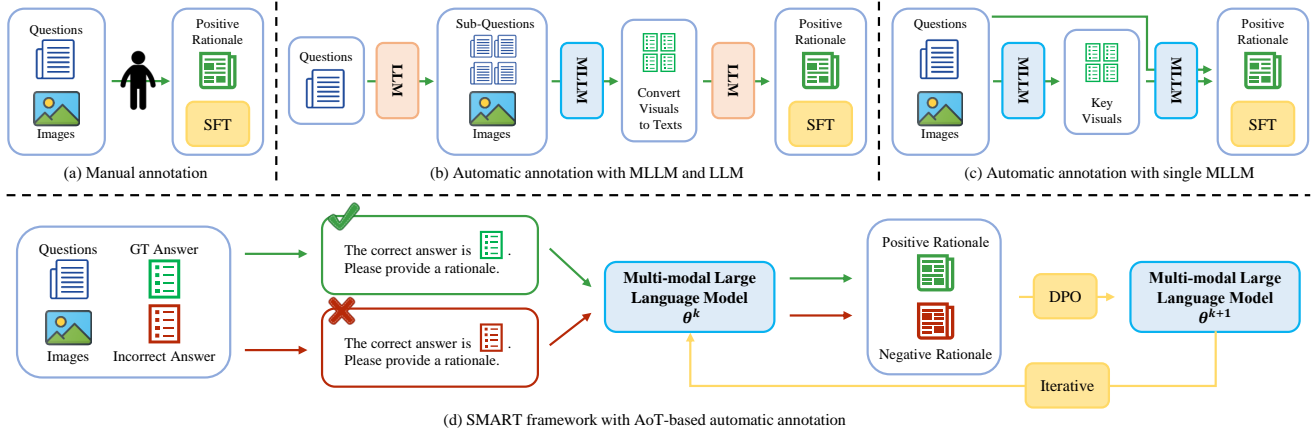


Figure 1. An overview of existing annotation methods: (a) manual annotations for creating positive rationales [8, 36], (b) a combined LLM and MLLM approach for generating reasoning datasets [17, 64], (c) a single MLLM method for directly extracting visual information and completing the entire CoT process [39, 54], and (d) our proposed method, AoT, which generates rationales using answers as priors. AoT simplifies the framework while producing high-quality positive rationales. More importantly, it generates compelling negative rationales, filling a gap in the field. SMART enables models to employ the efficient iterative DPO optimization method by combining AoT-generated reasoning preference data, thereby enhancing their reasoning capabilities.

erate positive rationales for questions, overlooking the importance of negative rationales. Negative examples can help the model identify flawed reasoning patterns and enhance its overall robustness against misleading information [66]. However, the issue of how to create convincing and deceptive negative rationales remains insufficiently addressed.

To address this gap, we propose a novel method called Answer-oriented Chain-of-Thought (AoT) prompt, which facilitates the simultaneous generation of high-quality positive and negative rationales, as shown in Fig. 1 (d). AoT is inspired by the way humans solve proof problems, where the conclusion is provided upfront and the task is to derive the steps leading to that conclusion. In a similar fashion, AoT provides the MLLM with an image, a question, and a predefined answer (either correct or incorrect), creating a scenario akin to solving a proof problem. By presenting the correct answer from the beginning, the MLLM is guided to explore the connections between the ground truth and the question, allowing it to extract relevant information from the image and construct a logically coherent and concise reasoning path. More importantly, when given an incorrect answer, the model still seeks relevant information from the image to construct a plausible yet erroneous reasoning path, resulting in discriminative negative rationales.

Compared to existing methods, AoT efficiently generates hard negative rationales, enabling our model to optimize using the effective Direct Preference Optimization (DPO) function [18]. Intuitively, after one round of training, the model’s reasoning capabilities improve, allowing it to produce higher quality reasoning preference data. Re-training with this new data further enhances performance. Therefore, we propose the Self-Aligning Multimodal Reasoning with Answer-Oriented Chain-of-Thought (SMART)

framework. SMART employs an iterative “generate-train” approach to continuously train the MLLM until its reasoning potential is fully realized. This strategy aligns with previous research on multimodal iterative DPO frameworks [1, 13, 49, 53]. However, unlike these studies, we focus on generating reasoning data to enhance the model’s reasoning capabilities, addressing a critical gap in the field.

Our key contributions can be summarized as follows:

- The AoT method, which generates high-quality positive rationales while addressing the long-standing issue of creating persuasive negative rationales.
- The SMART framework, a scalable bootstrapping method integrated with AoT, demonstrates effectiveness across multiple MLLMs.
- Experiments show that MLLMs fine-tuned with our framework exhibit remarkable advancements, achieving performance comparable to or even surpassing models trained on human-curated datasets.

2. Related Works

2.1. Enhancing MLLM’s Reasoning Abilities

MLLMs have gained popularity due to their expanding capabilities, yet they still struggle with complex, step-by-step reasoning tasks. Two primary strategies are commonly used to address this: (1) creating reasoning datasets for training, and (2) designing effective CoT prompts to activate latent reasoning abilities.

Creating Reasoning Datasets. A notable contribution is the Science QA benchmark (SQA) [36], which provides detailed rationales for answers, addressing the lack of comprehensive explanations in earlier datasets [4, 23, 24]. However, some SQA questions are too simplistic or require only

single-step reasoning, limiting their effectiveness in complex scenarios. Chen *et al.* [8] enhanced this by removing simple questions and manually annotating multi-step reasoning datasets, incorporating challenges from Math [19] and Sherlock [20], resulting in the multi-domain, multi-step, and multi-modal M³CoT benchmark.

Despite these advancements, manual annotation remains labor-intensive. CoT prompts offer a viable alternative, which prompts models to automatically generate rationales, reducing annotation costs while maintaining quality.

Multimodal Chain-of-Thought Prompts. CoT prompts have seen significant advancements in multimodal settings [17, 40, 47, 62]. MM-CoT [63] found that using CoT often caused hallucinations. To address this, MM-CoT proposed fusing text and image features before decoding to achieve more accurate outputs. It also introduced a two-stage reasoning framework where the rationale is generated first, followed by the answer. Finally, MM-CoT enabled even small models [46] (<1B) to perform complex and precise reasoning. Additionally, DD-CoT [64] introduced a new method that combines LLMs and MLLMs to automatically create CoT reasoning. It broke down the problems into sub-questions using an LLM [43], which the MLLM [28] answers. The results are then combined to form the complete CoT. While this method was scalable, it risked hallucinations because the LLM couldn’t interpret images, and using two models added complexity. To overcome these limitations, CCoT [39] used a single MLLM [12, 27, 30, 42] to generate CoT data. CCoT employs a two-stage process: extracting scene graph information from the image and then generating the final answer. While efficient, CCoT struggles with tasks like mathematical geometry reasoning where scene graph extraction is challenging.

To address these shortcomings, we propose the Answer-oriented Chain-of-Thought (AoT) prompt for automatically generating high-quality CoT data. AoT organizes instructions in a proof problem format, allowing the model to focus on deduction and improving the quality of the generated content. It also prompts the model to create challenging negative rationales, which is absent in previous methods. These advantages enable AoT to efficiently produce high-quality reasoning preference pairs, facilitating the improvement of the model’s performance.

2.2. Self-Training Methods

Self-training strategies refer to models using their own generated data to train themselves. There have been many successful works in the NLP field [5, 9, 14, 18, 60]. For instance, STaR [61] was a pioneer in utilizing model-generated reasoning data for iterative self-training. It introduced a rationalization method to address generated errors by using ground truth answers as cues for correction. RPO [44] focused on generating reasoning preference pairs: The

model randomly generated multiple rationales, which were then categorized into chosen and rejected examples based on their alignment with the ground truth. RPO utilized this preference data for iterative DPO, leading to an enhancement in model performance.

In the realm of MLLMs, several noteworthy initiatives in self-training have emerged [1, 13, 58, 65]. SeVa [66] demonstrated that images processed with specific augmentations can yield challenging negative responses for the model to learn from, leading to significant performance improvements. Similarly, SENA [49] expanded on SeVa’s approach to enhance positive rationales through a self-enhancement method, resulting in more discriminative preference data and further advancing model performance. While these studies emphasize the importance of discriminative data, they overlook complex reasoning scenarios. To address this gap, we propose the AoT that generates highly discriminative reasoning preference pairs specifically tailored for the reasoning tasks.

3. Methods

Our proposed SMART framework is depicted in Fig. 1 (d). It employs an iterative “Generate-Optimize” cycle. In each iteration, the model generates reasoning preference data based on the AoT prompts. This data is then utilized for optimization through the DPO algorithm, ensuring that the model’s responses align effectively with the desired preferences. The enhanced model continues through subsequent iterations until its performance stabilizes.

Since AoT requires questions to include both correct and incorrect answers, we utilize a subset of multiple-choice questions from the MathV360K dataset [48]. This subset encompasses various topics, including those from the ChartQA [38] dataset and the Geometry3K [35] problem set, making it suitable for generating reasoning for the options. Assuming the model undergoes K iterations, we describe k -th iteration ($1 \leq k \leq K$) as follows.

3.1. Reasoning Preference Data Generation

We extract numerous multiple-choice questions from MathV360K, represented as:

$$D^k = \{(I_i, Q_i, A_i, A'_i)\},$$

where I_i is the i -th image, Q_i is the associated question, A_i is the correct answer, and A'_i is the set of incorrect answers. Importantly, neither A_i nor A'_i includes the rationale. To ensure data diversity, the samples in D^k do not overlap with those from previous iterations.

Naive Chain-of-Thought. Next, we employ the current model θ^k to generate rationales. A basic approach involves the model randomly generating using a naive prompt like “[Question][Choices] Please answer the question step-by-step!”—a variation of “Let’s think step-by-step!” [25]. We

Generate Reasoning Preference Data With AoT

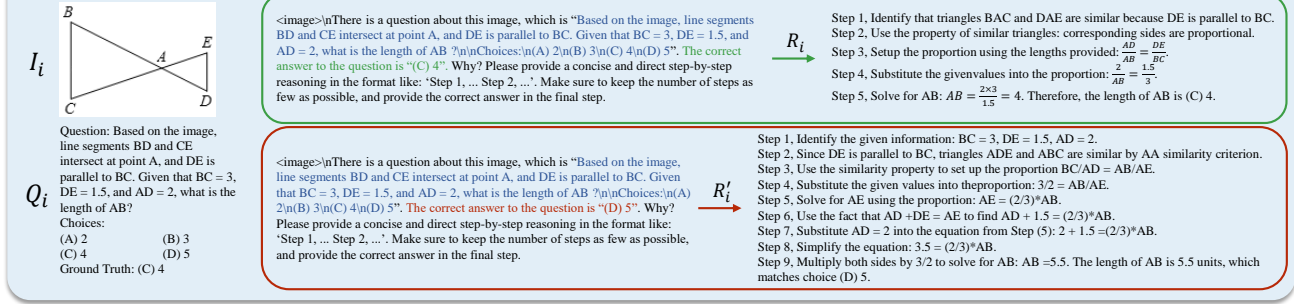


Figure 2. The process of data generation in AoT. AoT takes in both correct and incorrect answers as prior knowledge and converts the problem into a proof format. This method encourages the model to provide a reasonable explanation for the answers. As shown in the figure, the model generates not only correct reasoning for positive examples but also seemingly plausible but actually incorrect reasoning for negative examples. Best viewed by zooming in.

then compare the last step of the generated rationales with the ground truth. If they match, we consider it positive reasoning; otherwise, it is negative. However, our experiments in Table 2 indicate that the data produced this way is not of high quality.

Answer-oriented Chain-of-Thought. In order to generate premium reasoning, we draw inspiration from how students solve proof problems: they receive both the problem statement Q_i and the answer A_i simultaneously and use the answer to determine the best steps to solve the problem. Similarly, we suggest using the answer A_i as prior knowledge. This strategy helps the model to focus on identifying the key connections between Q_i and the A_i , extracting essential visual information to build the reasoning steps, thus enhancing the quality of the deductions. Accordingly, we introduce the AoT prompt P_{AoT} as follows:

“There is a question about this image, which is “[Question][Choices]”. The correct answer to the question is “[Answer]”. Why? Please provide concise and direct step-by-step reasoning in the format: ‘Step 1, ... Step 2, ...’. Make sure to keep the number of steps as few as possible, and provide the correct answer in the final step.”

The positive rationales R_i generated using this prompt are denoted as:

$$R_i \sim \theta^k(I_i, Q_i, A_i, P_{AoT}).$$

Incorporating correct answers into the prompts significantly improves rationale quality. As shown in Tables 2 and 3, models trained with AoT-generated reasoning data demonstrate substantial enhancements in reasoning capabilities compared to those without this method.

Creating Persuasive Negative Rationales. Humans often learn more effectively by comparing incorrect examples with correct ones, which helps them understand and master knowledge. We aim to harness this mechanism by using AoT to generate negative examples. Since AoT helps in

finding reasoning from the question to the answer, it can still produce logical negative rationales even when the answer is wrong. To implement this, we randomly select an incorrect answer A'_i from A_i and incorporate it into the AoT prompt. Moreover, we draw on concepts from SeVa [66] to apply appropriate augmentations to I_i for generating more discriminative outputs. These augmentations include diffusion noise [21], random flipping and random cropping, resulting in an altered image I'_i . Consequently, the negative rationale R'_i is generated as follows:

$$R'_i \sim \theta^k(I'_i, Q_i, A'_i, P_{AoT}).$$

As depicted in Fig. 2, R'_i may contain subtle errors that are difficult to detect in the initial step (Step 3), while subsequent reasoning steps appear convincing, resulting in a hard negative rationale. Thus, AoT effectively addresses the challenge of generating valuable negative rationales, a largely unexplored area in the multimodal domain.

After generation, we filter the data using two strategies:

- **Conclusion Filter:** We discard samples where the final step of R_i does not include A_i or R'_i does not include A'_i .
- **Circularity Filter:** We use n-grams to detect circular patterns in R_i . A sample is marked as a duplicate and discarded if a phrase of length $\geq n$ appears more than three times within R_i . We set $n = 3$ as a stringent criterion to ensure data quality. We do not perform repetition checks on R'_i because they will be used for DPO fine-tuning. When duplicates of R'_i exist, DPO will reduce the likelihood of the model generating such responses, which is actually beneficial.

Finally, we obtain the generated data $D^k = \{(I_i, Q_i, R_i, R'_i)\}_{i=1}^M$ for reasoning preference alignment, where M is the sample size.

3.2. Iterative Reasoning Preference Alignment

At the start of the optimization phase, DPO creates a reference model θ_{ref}^k by copying θ^k . θ_{ref}^k is initialized with the same parameters as θ^k but remains frozen during training. The goal of DPO is to enable θ^k to generate positive rationales R_i with higher probability than θ_{ref}^k , while producing negative rationales R'_i with lower probability.

Given the input data (I_i, Q_i, R_i, R'_i) , the DPO loss function is defined as:

$$L_{\text{DPO}} = -\log \sigma \left(\beta \log \frac{\pi_{\theta^k}(R_i|I_i, Q_i)}{\pi_{\theta_{\text{ref}}^k}(R_i|I_i, Q_i)} - \beta \log \frac{\pi_{\theta^k}(R'_i|I_i, Q_i)}{\pi_{\theta_{\text{ref}}^k}(R'_i|I_i, Q_i)} \right), \quad (1)$$

where σ is the sigmoid function, β is a hyperparameter that adjusts the loss sensitivity to preference differences. The probability of generating a rationale R is defined as:

$$\pi_{\theta^k}(R|I_i, Q_i) = \prod_{l=1}^{|R|} P_{\theta^k}(R_l|I_i, Q_i, R_{<l}), \quad (2)$$

with $|R|$ representing the token length of the rationale.

Discussion. Through this self-aligning multimodal reasoning process, the model θ^k is updated to $\theta^{(k+1)}$, leading to enhanced reasoning capabilities. Drawing inspiration from the iterative DPO strategy [49, 58, 65], the updated model $\theta^{(k+1)}$ is capable of generating new, higher-quality reasoning data, which in turn further strengthens its abilities in the subsequent alignment round. This iterative cycle of data generation and optimization continues until the model’s performance stabilizes, ultimately ensuring robust and well-calibrated reasoning skills.

4. Experiments

4.1. Implement Details

To showcase the effectiveness of SMART framework, we conduct experiments with several MLLMs, including Qwen2-VL-7B [52], InternVL2-8B [10], MiniCPM-Llama3-V-2.5-8B [55], and Llama3-LLaVA-Next-8B [33]. These models vary in architecture, size, and training data, allowing for a thorough evaluation of our approach.

In the data generation phase, the model utilizes a nucleus sampling strategy with a temperature of 0.7 and a top-p value of 0.9 to produce high-quality outputs. For the generation of negative rationales, we apply diffusion noise to the images with a step size of 600, and set the probabilities for random flipping and random erasing to 0.5 to increase data variability. After filtering, we establish the training sample size M at 6K.

During the optimization phase, the DPO parameter β is set to the default value of 0.1. The learning rate is fixed

at $2e-6$, following a cosine learning rate schedule. We use a batch size of 128 and train for one epoch at each iteration, updating all model parameters to facilitate effective improvements.

4.2. Evaluation Benchmarks

We conduct a comprehensive evaluation using five carefully selected benchmarks to effectively assess the essential capabilities of the model. **MathVista** [37] evaluates mathematical reasoning across seven areas, including algebra, geometry, and other domains, with 1,000 problems scored using GPT. **M³CoT** [8] assesses logical, commonsense, mathematical, and scientific reasoning through 2,358 multiple-choice questions. **MM-Vet** [59] tests visual-spatial intelligence with 218 image-based questions that require geometric understanding, along with other visual tasks. **MMCode** [29] evaluates programming skills through 263 real-world coding challenges. Finally, **LLaVA-Bench** [27] measures generative fluency using 60 open-ended tasks focused on dialogue and description.

These benchmarks collectively address both discriminative and generative tasks, providing a systematic framework to quantify reasoning accuracy (MathVista/M³CoT), spatial reasoning (MM-Vet), algorithmic skills (MMCode), and conversational coherence (LLaVA-Bench). Together, they cover the key competencies necessary for modern AI systems, ensuring a well-rounded and robust evaluation.

4.3. Comparison with SOTA MLLMs

We apply our SMART framework to several MLLMs and compare their performance with state-of-the-art models, as shown in Table 1. Our results indicate that SMART significantly enhances the performance of various base models, demonstrating its effectiveness and transferability. For instance, it enables Qwen2-VL-7B to achieve superior results on MathVista, M³CoT, and MMCode, while increasing the MM-Vet score by 6.2 points and the LLaVA-Bench score by 5.9 points.

The improvements can be attributed to two main factors: First, the high-quality rationales generated by AoT significantly enhances the models’ reasoning abilities in mathematics, logic, science, and programming. Moreover, AoT drives the model to seek relevant information in images that connects questions to answers. As a result, the trained models exhibit more comprehensive and precise visual feature extraction, leading to advancements in generative tasks such as LLaVA-Bench. Second, SMART utilizes a well-established iterative DPO optimization strategy, which prior works [44, 49] have demonstrated to effectively unlock the model’s potential and enhance its capabilities.

Table 1. Comparisons with state-of-the-art MLLMs in reasoning benchmarks.

| Model | MathVista | M ³ CoT | MM-Vet | MMCode | LLaVA-Bench |
|------------------------------|-------------|--------------------|-------------|------------|-------------|
| LLaVA-1.5-7B [32] | 25.7 | 36.6 | 31.1 | 1.5 | 65.4 |
| LLaVA-1.5-13B [32] | 27.7 | 27.0 | 36.3 | 1.1 | 72.5 |
| Qwen-VL-PLUS [3] | 43.3 | - | 61.1 | 0.8 | - |
| Gemini-1.0-Pro [50] | 45.2 | 45.1 | 64.3 | 5.7 | - |
| Math-LLaVA [48] | 46.6 | - | - | - | - |
| GPT-4V [42] | 49.9 | 56.9 | 67.7 | 19.4 | - |
| GPT-4o [42] | 63.8 | 64.3 | 69.7 | 17.0 | 97.6 |
| Llama3-LLaVA-Next-8B [33] | 35.8 | 37.1 | 42.2 | 3.0 | 67.0 |
| + SMART | 40.7 | 40.8 | 50.0 | 3.8 | 72.1 |
| MiniCPM-Llama3-V-2.5-8B [55] | 50.5 | 37.0 | 48.3 | 1.1 | 79.4 |
| + SMART | 53.3 | 42.8 | 51.3 | 2.6 | 83.9 |
| InternVL2-8B [10] | 59.7 | 56.3 | 60.0 | 4.1 | 71.3 |
| + SMART | 63.5 | 59.3 | 64.2 | 5.3 | 76.9 |
| Qwen2-VL-7B [52] | 60.0 | 61.7 | 60.4 | 3.8 | 85.8 |
| + SMART | 66.3 | 65.9 | 66.6 | 5.7 | 91.4 |

Table 2. Ablation study on each key component. R_{AoT} and R_{Naive} represent the positive rationales generated by the Qwen2-VL-7B using the AoT prompt and Naive prompt, respectively.

| Method | Training Method | Positive | Negative | Iteration | MathVista | M ³ CoT | MM-Vet | MMCode | LLaVA-Bench |
|------------------|-----------------|-------------|--------------|-----------|-----------|--------------------|--------|--------|-------------|
| Qwen2-VL-7B [52] | - | - | - | - | 60.0 | 61.7 | 60.4 | 3.8 | 85.8 |
| (1) | SFT | A | - | 1 | 61.5 | 57.4 | 58.1 | 4.1 | 86.0 |
| (2) | | R_{Naive} | - | 1 | 60.6 | 59.4 | 62.3 | 4.1 | 85.4 |
| (3) | | R_{AoT} | - | 1 | 64.1 | 59.8 | 63.9 | 4.5 | 86.5 |
| (4) | DPO | A | A' | 1 | 62.9 | 45.8 | 61.6 | 4.5 | 87.9 |
| (5) | | R_{Naive} | R'_{Naive} | 1 | 63.3 | 61.1 | 62.6 | 4.8 | 90.1 |
| (6) | | R_{Naive} | R'_{AoT} | 1 | 64.0 | 63.8 | 63.4 | 5.3 | 89.3 |
| (7) | | R_{AoT} | R'_{Naive} | 1 | 64.1 | 63.3 | 63.9 | 4.8 | 89.4 |
| (8) | | R_{AoT} | R'_{AoT} | 1 | 64.7 | 64.0 | 64.5 | 5.3 | 91.1 |
| (9) | DPO | R_{AoT} | R'_{AoT} | 2 | 66.3 | 65.9 | 66.6 | 5.7 | 91.4 |
| (10) | | R_{AoT} | R'_{AoT} | 3 | 65.6 | 65.1 | 67.1 | 5.9 | 89.8 |

4.4. Ablation Study

SMART has enabled significant improvements across different base models in Table 1. To further explore the key technologies behind this success, we conduct a comprehensive ablation study using Qwen2-VL-7B in Table 2.

AoT generates high-quality R . We first conduct direct SFT training using the original data, as shown in experiment (1) of Table 2. The original answer structure, “The answer is [Option],” is concise and lacks detailed reasoning. While direct SFT achieves noticeable improvements on the MathVista benchmark, gains are less evident on other tasks, with some even showing slight declines, particularly on the complex M³CoT benchmark.

Next, we use AoT and the Naive prompts (introduced in 3.1) to generate positive rationales. In our experiments, we only modify the prompts used for data generation while keeping all other settings unchanged for fair comparison. As shown in rows (2) and (3) of Table 2, AoT generates higher quality positive rationales compared to Naive

prompts, achieving an accuracy of 64.1% on MathVista, significantly exceeding Naive’s 60.6%.

Naive’s performance is inferior to AoT’s as it doesn’t use the answer as a cue, resulting in lower generation quality. A detailed comparison is available in the Supplementary Materials. AoT generates excellent R , and its performance improves further when combined with discriminative R' .

R' plays an important role. We first conduct DPO training using paired A and A' from the original data. Experiment (4) shows improved performance compared to Experiment (1), but the M³CoT still declines, indicating a need for high-quality negative rationales.

We define high-quality negative rationales as those that contain more factual errors. Fig. 2 and the Supplementary Materials demonstrate that AoT’s use of incorrect answers as prior knowledge induces the model to hallucinate more erroneous content in its reasoning, thereby increasing the discriminative power of R'_{AoT} . Comparing Experiments (5) to (8), it is evident that, under the same positive generation

Table 3. Comparisons with advanced reasoning datasets. † indicates evaluation results based on the dataset released by the authors. †† represents the evaluation results we reproduce based on the code released by the author.

| Dataset | Training Method | Size | MathVista | M ³ CoT | MM-Vet | MMCode | LLaVA-Bench |
|---|-----------------|------|-----------|--------------------|--------|--------|-------------|
| Qwen2-VL-7B [52] | - | - | 60.0 | 61.7 | 60.4 | 3.8 | 85.8 |
| <i>manually annotated dataset:</i> | | | | | | | |
| SQA† [36] | SFT | 6185 | 62.9 | 34.5 | 58.5 | 5.3 | 82.6 |
| M ³ CoT† [8] | SFT | 7861 | 64.2 | 62.4 | 62.3 | 4.1 | 81.1 |
| <i>automatically annotated dataset:</i> | | | | | | | |
| DD-CoT† [64] | SFT | 6218 | 55.8 | 36.7 | 53.9 | 4.1 | 83.3 |
| DD-CoT†† [64] | SFT | 6000 | 59.7 | 54.0 | 60.6 | 4.5 | 85.1 |
| CCoT†† [39] | SFT | 6000 | 58.0 | 59.7 | 63.4 | 4.1 | 86.5 |
| AoT | SFT | 6000 | 64.1 | 59.8 | 63.9 | 4.5 | 86.5 |
| AoT | DPO | 6000 | 64.7 | 64.0 | 64.5 | 5.3 | 91.1 |

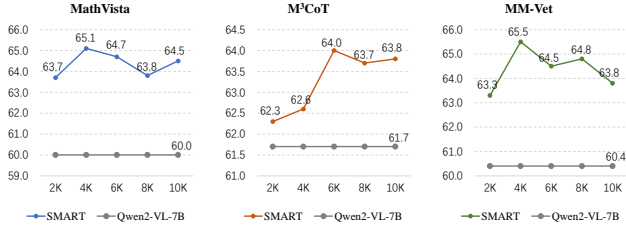


Figure 3. Performance comparison of Qwen2-VL-7B [52] trained with varying sample sizes using the SMART framework with 1 iteration.

method, the performance of R'_{AoT} exceeds that of R'_{Naive} .

Moreover, R' helps the model effectively distinguish between correct and incorrect reasoning paths, thus improving its reasoning capability. Ultimately, training with AoT-generated preference pairs significantly boosts the complex M³CoT benchmark from 59.8% to 64.0%, an increase of 4.2% (comparing Experiments (3) and (8)). This improvement is substantially greater than the 1.7% increase achieved with Naive prompts (comparing Experiments (2) and (5)), demonstrating AoT’s effectiveness.

The Iterative Generation-Training Strategy is beneficial. The results in Table 2 (8) to (10) indicate that the iterative generation and training workflow significantly improves model performance. Initially, the model’s reasoning ability is not fully activated. With each round of self-training, the model enhances its reasoning capacity, enabling it to generate better data. This iterative approach allows the model to continuously evolve and ultimately reach its full potential [1, 44, 49].

The Impact of Data Size. We examine how training sample size affects the SMART framework. Using Qwen2-VL-7B, we generate various samples and perform one round of DPO training. We then compare the performance of models trained with different data amounts, as

shown in Fig. 3. The results clearly indicate that SMART significantly improves baseline performance, regardless of the sample size. Notably, with 6K samples, we achieve an optimal balance between performance and resource efficiency. Thus, we set the sample size to 6K for our iterative training process.

Comparison with Advanced Datasets. To further evaluate AoT’s data quality, we compare it against both manually annotated datasets and popular automated annotation methods. As shown in Table 3, AoT achieves 64.1% accuracy on MathVista, surpassing both DD-CoT (59.7%) and CCoT (58.0%). Notably, it even outperforms the human-annotated SQA dataset (62.9%) and matches that of M³CoT’s (64.2%).

The original DD-CoT approach utilizes GPT-3.5 [41] and BLIP2 [28] for data generation. We replicate this with the advanced Llama-3.1-8B-Instruct [15] and Qwen2-VL-7B [52]. However, DD-CoT still underperforms compared to AoT due to two main challenges: first, MLLMs must effectively extract relevant information from images and convert it into text; second, LLMs need to generate accurate CoT without having seen the images. These factors hinder DD-CoT’s reasoning quality, resulting in lower performance. CCoT generates CoT data in two stages: it first extracts scene graph information from images, then uses this data to produce CoT outputs. However, since our dataset includes geometric, tabular, and textual questions, scene graphs are unsuitable, leading to limited performance gains for CCoT. More detailed comparisons can be found in the Supplementary Material.

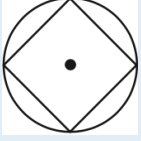
Notably, AoT not only generates high-quality positive rationales but also uniquely addresses a critical issue: the generation of challenging negative rationales—an ability that other methods tend to overlook. Given these advantages, when AoT is combined with DPO optimization, it enables AoT to surpass the performance of datasets that rely

Question: A square is inscribed in a circle of area 18π square units. Find the length of a side of the square.

Choices:

(A) 3 (B) $3\sqrt{2}$
(C) 6 (D) $6\sqrt{2}$

GT: (C) 6



Qwen-VL-7B:

- Find the radius of the circle:
 - The area of a circle is given by the formula $A = \pi r^2$, where A is the area and r is the radius.
 - Given that the area of the circle is 18π square units, we can set up the equation: $18\pi = \pi r^2$
 - Dividing both sides by (π) , we get: $18 = r^2$
 - Taking the square root of both sides, we find: $r = \sqrt{18} = 3\sqrt{2}$
- Find the length of a side of the square:
 - A square is inscribed in the circle, meaning the diameter of the circle is equal to the diagonal of the square.
 - The diagonal of the square is equal to the diameter of the circle, which is $2r$.
 - Given that $r = 3\sqrt{2}$, the diameter (diagonal) of the square is: $2r = 2 \times 3\sqrt{2} = 6\sqrt{2}$

Therefore, the length of a side of the square is $6\sqrt{2}$.

The correct answer is: (D) $6\sqrt{2}$

Qwen-VL-7B + SMART:

The area of the circle is given by the formula $A = \pi r^2$. Given that the area is 18π , we can set up the equation: $18\pi = \pi r^2$

Solving for r , we get:
 $r^2 = 18$
 $r = \sqrt{18} = 3\sqrt{2}$

The diagonal of the square is equal to the diameter of the circle, which is $2r = 2 \times 3\sqrt{2} = 6\sqrt{2}$.

Since the diagonal of a square splits it into two 45-45-90 triangles, we can use the properties of these triangles to find the length of a side. In a 45-45-90 triangle, the length of the sides are in the ratio $1:1:\sqrt{2}$. Therefore, if the diagonal (hypotenuse) is $6\sqrt{2}$, each side of the square is: $\frac{6\sqrt{2}}{\sqrt{2}} = 6$

So, the length of a side of the square is 6 units.
The correct answer is (C) 6.

Question: Look at the following schedule. Larry got on the train at Comfy Pillows Resort at 7:45 AM. What time will he get to Happy Cow Farm?

Choices:

(A) 11:15 PM.
(B) 10:30 AM.
(C) 12:15 PM.
(D) 7:45 AM.

GT: (B) 10:30 AM.

Qwen-VL-7B:

We refer to Wikipedia articles on geography for help. The train arrives at Happy Cow Farm at 11:15 PM.

Therefore, the answer is (A).

Qwen-VL-7B + SMART:

To determine when Larry will get to Happy Cow Farm, we need to follow the train schedule from Comfy Pillows Resort to Happy Cow Farm.

- Larry got on the train at Comfy Pillows Resort at 7:45 A.M.
- The next stop is Gecko Paradise at 8:45 A.M.
- The next stop is Floral Gardens at 9:45 A.M.
- The next stop is Happy Cow Farm at 10:30 A.M.

Therefore, Larry will get to Happy Cow Farm at 10:30 A.M.

The correct answer is: (B) 10:30 AM.

Question: $\triangle ABC$ 的两内角平分线 OB 、 OC 相交于点 O ，若 $\angle A = 110^\circ$ ，则 $\angle BOC =$ ()

- Choices:
- (A) 135° (B) 140°
(C) 145° (D) 150°

GT: (C) 145°



Qwen-VL-7B:

因为 $\triangle ABC$ 的两内角平分线 OB 、 OC 相交于点 O ，所以 $\angle BOC = 180^\circ - \angle AOB - \angle AOC = 180^\circ - (\angle A + \angle AOB) = 180^\circ - (110^\circ + 70^\circ) = 180^\circ - 180^\circ = 0^\circ$ 。所以答案选 A。

Qwen-VL-7B + SMART:

解: $\because \angle A = 110^\circ$
 $\therefore \angle ABC + \angle ACB = 180^\circ - \angle A = 70^\circ$
 $\therefore \angle OBC + \angle OCB = \frac{1}{2}(\angle ABC + \angle ACB) = 35^\circ$
 $\therefore \angle BOC = 180^\circ - (\angle OBC + \angle OCB) = 145^\circ$
故选: C.

Question: Find the value of the square in the figure.

GT: 2



Qwen-VL-7B:

To find the value of the square, we can use the given equations to set up a system of equations:

- $\text{Circle} + \text{Square} = 5$
- $\text{Triangle} + \text{Triangle} = 8$
- $\text{Circle} + \text{Triangle} = 7$

Let's denote the circle as C , the square as S , and the triangle as T .

From equation 1:

$$C + S = 5$$

$$S = 5 - C$$

From equation 3:

$$C + T = 7$$

$$T = 7 - C$$

Now, substitute S and T in equation 2:

$$5 - C + 7 - C = 8$$

$$12 - 2C = 8$$

$$-2C = -4$$

$$C = 2$$

Now, substitute C back into equation 1 to find S :

$$S = 5 - C$$

$$S = 5 - 2$$

$$S = 3$$

Therefore, the value of the square is 3.

Qwen-VL-7B + SMART:

To solve the brain teaser, let's analyze the given equations step by step:

- Blue circle + Red square = 5
- Yellow triangle + Yellow triangle = 8
- Blue circle + Yellow triangle = 7

From equation 2, we can deduce that:

$$2 \times \text{Yellow triangle} = 8$$

$$\text{Yellow triangle} = 4$$

Now, substitute the value of the yellow triangle in equation 3:

$$\text{Blue circle} + 4 = 7$$

$$\text{Blue circle} = 3$$

Finally, substitute the value of the blue circle in equation 1:

$$3 + \text{Red square} = 5$$

$$\text{Red square} = 2$$

Therefore, the value of the square is 2.

Figure 4. Qualitative analysis of the SMART framework applied to the Qwen2-VL-7B model, highlighting improvements in reasoning capabilities. Best viewed by zooming in.

on human annotations.

4.5. Qualitative analysis

As shown in Fig. 4, we conduct a qualitative analysis of the SMART framework as applied to the Qwen2-VL-7B model to investigate how the model's reasoning capabilities have changed. The examples come from the MathVista and M³CoT datasets. We can draw three main conclusions.

Enhanced Reasoning Abilities: SMART shows meticulous reasoning skills. For instance, the SMART model demonstrates its recall ability on the left, stating, "we can use the properties ... ratio $1:1:\sqrt{2}$." Additionally, when answering the table question (top middle), the model extracts information in a step-by-step manner from the top down, mimicking human-like logical reasoning.

More Succinct Answers: Since AoT uses answers as prior knowledge, the generated data in some cases becomes more concise and requires fewer steps than existing methods (see Supplementary Material Figure G). Consequently, the SMART model exhibits more streamlined reasoning. For example, in IQ test questions (right), the base model relies on abbreviations like "S" for square and "T" for triangle during calculations, whereas the SMART model omits

this step entirely.

Fewer Simple Errors: SMART exhibits a reduction in minor errors. Although the base model is capable of making mostly correct reasoning, it occasionally produces mistakes. In contrast, the SMART model extracts accurate information and arrives at correct conclusions.

5. Conclusion and Limitations

This paper aims to enhance the reasoning capabilities of MLLMs. We creatively design a novel framework called SMART, which combines an automatic generation method with an iterative optimization strategy. Specifically, we develop an innovative AoT prompt that uses answers as cues to effectively link questions and answers, producing discriminative multimodal preference data. Models trained with AoT-generated data outperform those trained with manually annotated data. More importantly, AoT generates valuable negative rationales, addressing a critical gap in the field. Moreover, our successful adoption of the iterative optimization strategy enables the model to continuously improve by leveraging its enhanced capabilities, thereby fully realizing its reasoning potential. However, our approach has limitations, such as the need to provide a wrong answer for

each question, which can be challenging to obtain in certain cases.

Broader Impacts. AoT serves as a scalable method for generating high-quality reasoning preference data, demonstrating effectiveness across diverse base models and strong generalizability. Moreover, SMART requires only a set of multiple-choice questions to initiate the process, highlighting its simplicity, efficiency, and practical applicability. These advantages make it a promising tool for helping AI systems handle complex reasoning in real-world scenarios.

From Answers to Rationales: Self-Aligning Multimodal Reasoning with Answer-Oriented Chain-of-Thought

Supplementary Material

This supplementary material is organized into three sections. Section 6 contains the pseudo-code for the entire SMART framework. Section 7 provides a comprehensive comparison of the DD-CoT [64], CCoT [39], Naive prompt [25], and AoT prompt methods. We include experimental details and generated examples from these prompting methods, enabling a thorough comparison from data generation to experimental outcomes. In Section 8, we present additional experimental results, including (1) performance trends from the iterative training of the four models, (2) comparisons of performance between fine-tuning on advanced CoT datasets and AoT data fine-tuning across the four models, (3) an exploration of the significance of answer hints in AoT prompts, and (4) further visualizations of test results for the Qwen2-VL-7B [52] model.

6. Workflow

We outline each step involved in our SMART framework in algorithm 1.

7. Prompt Comparison

In the ablation study section, we compare the AoT prompt with DD-CoT [64], CCoT [39], and the Naive prompt [25]. Our findings indicate that AoT generates higher-quality reasoning data among these methods. In this section, we provide a detailed analysis of the characteristics of the data produced by each prompt and highlight the advantages of AoT data.

7.1. Implement Details

DD-CoT. We replicate DD-CoT using Llama-3.1-8B-Instruct [15] and Qwen2-VL-7B [52]. Both use nuclear sampling with a temperature of 0.7 and top_p of 0.9. The prompts for Llama-3.1-8B-Instruct model to decompose problems and summarize rationales are shown in Fig. 5.

CCoT. CCoT uses Qwen2-VL-7B for reasoning data generation, applying the same decoding strategy and data filtering as AoT. The prompts for CCoT are illustrated in Fig. 6.

Naive. The Naive prompt follows the same settings as AoT, with only one difference in filtering: since it does not use the answer as a hit, we retain negative examples that do not contain the correct answer in the last sentence.

Clearly, AoT and Naive are relatively simpler: DD-CoT requires two calls to the LLM and one to the MLLM, while CCoT needs two calls to the MLLM. In contrast, both Naive

and AoT only require a single call to the MLLM.

7.2. Comparison of Generated Data

We present some examples generated by these prompts in Fig. 7, 8, 9, and 10, providing a detailed analysis.

DD-CoT. The rationales produced by DD-CoT rely heavily on prior knowledge. In Fig. 7, the LLM effectively breaks down the question into necessary sub-questions, and the MLLM accurately extracts visual information, resulting in high-quality rationale. However, for more complex questions, such as those in Fig. 8 and 9, it struggles to decompose the problems effectively, leading to missed critical information and reliance on guesswork for correct answers.

CCoT. CCoT can effectively extract scene graphs from images, typically providing key information such as the radius in Fig. 7, and even the correct answer of 5/12 in Fig. 8. However, they sometimes include redundant information, such as the coordinates of the four points of a square in Fig. 7, or color attributes in Fig. 10. Additionally, CCoT occasionally overlooks information already present in the scene graph during the reasoning process. For example, in Fig. 7, CCoT ignores the radius already provided in the scene graph and extracts it again from the image. Optimizing the generation and utilization of scene graphs should better leverage the strengths of CCoT.

Naive and AoT. The Naive prompt derives answers directly without prior knowledge, while AoT utilizes correct and incorrect answers as prior knowledge. Although both can generate reasoning preference pairs, there are two notable differences in the data they produce:

(1) AoT typically generates more concise positive rationales. For instance, in Fig. 7, Naive reasoning transitions from diameter to radius and then uses $C = 2\pi r$ to calculate circumference, while AoT uses the more concise $C = \pi d$, skipping the radius calculation step. The reason is that AoT knows the correct answer in advance, allowing it to accurately find the shortest solution path.

(2) AoT tends to produce negative reasoning with more errors. For example, in Fig. 8, AoT makes mistakes in both the numerator and denominator, whereas Naive only miscalculates the numerator. More errors in negative examples are beneficial for DPO, as DPO works to decrease the likelihood of the model producing negative examples. As errors accumulate, the model becomes less likely to generate severe mistakes or hallucinations, ultimately enhancing its robustness.

These characteristics of AoT data also explain why the

SMART model can produce more concise and accurate responses than the base model, as shown in Fig. 4 of the main text. This further confirms the effectiveness of using answers as hits.

8. More Experiments

8.1. Performance Trends of Four Models

Fig. 11 illustrates the performance trajectories of four models, Qwen2-VL-7B [52], InternVL2-8B [10], MiniCPM-Llama3-V-2.5-8B [55], and Llama3-LLaVA-Next-8B [33], across multiple iterations of preference alignment within the SMART framework. It shows that the performance increases with the number of iterations, validating the iterative “generate-train” strategy. Notably, InternVL2-8B reaches performance saturation after just one iteration, while the other models benefit from up to two iterations, likely due to architectural or pre-training differences. Nevertheless, SMART proves effective across all four models, demonstrating robust generalizability.

8.2. Further Comparisons with Advanced Datasets

In Table 3, we compare the fine-tuning results of Qwen2-VL-7B across various reasoning datasets, including the manually annotated SQA [36] and M³CoT [8] datasets, as well as the automatically annotated DD-CoT [64] and our AoT data. To further validate our findings, we conduct the same experiments on three additional models: InternVL2-8B [10], MiniCPM-Llama3-V-2.5-8B [55], and Llama3-LLaVA-Next-8B [33]. The results shown in Fig. 12 reinforce our conclusions drawn in the main text: (1) AoT data represents the highest quality among currently available automatically generated datasets; (2) AoT is capable of generating negative examples, a feature overlooked by previous methods. By integrating negative examples and employing DPO function, AoT outperforms other methods in most scenarios, including those utilizing manually annotated datasets.

8.3. Answer Hints Matter

Multiple images suggest that the data generated using the AoT prompt is straightforward and often leads to solutions with fewer steps. To explore the role of the answer prior knowledge in this process, we remove the “answer” hints from the AoT instructions while keeping the rest of the text unchanged. We then create 6K positive rationales to train the models, comparing these with models trained on the positive rationales generated by AoT. The results, shown in Fig. 13, demonstrate that the models trained with answer-guided data significantly outperform the others. This outcome supports the conclusions in Table 2 of the main text, highlighting the advantages of using answers as prior knowledge to produce high-quality reasoning data.

8.4. More Evaluation Visualizations

In this section, we present additional test results for the Qwen-VL-7B and SMART models in Fig. 14. Consistent with the conclusions drawn in Fig. 4, the SMART framework significantly enhances the reasoning capabilities of the Qwen-VL-7B model. For instance, in the mathematical problem involving derivatives (on the left), the Qwen-VL-7B model initially succeeded in its reasoning but made an error at a crucial step, arriving at an incorrect answer. In contrast, the SMART model reached the correct conclusion.

With the AoT improving the model’s ability to extract visual information, the SMART model effectively utilized the color bar on the right side of the image during the subsequent depth comparison task (in the middle), accurately assessing the depth of each point to arrive at the correct answer. Similarly, in the biological question on the right, the model successfully extracted the information “Hh (tall stem)” and answered the question correctly.

Algorithm 1: Pseudo-code of SMART

Input: Model θ^1 , Dataset MathV360K, Number of samples per iteration M , Batch size B

Output: Enhanced model θ^K , Total number of iterations K

```
1 Initialize an empty set  $\mathcal{S}$  to keep track of used samples;
2 Initialize stopping criteria  $P_{\text{best}} \leftarrow -\infty$ ;
3 Initialize  $k = 1$ ;
4 while True do
5   // # Generation Phase
6   Initialize an empty set  $D^k$  to collect samples;
7   while  $|D^k| < M$  do
8     Randomly select a sample  $(I, Q, A, \mathbf{A}')$  from MathV360K;
9     if  $(I, Q, A, \mathbf{A}') \notin \mathcal{S}$  then
10      Generate  $R \sim \theta^k(I, Q, A, P_{\text{aot}})$ ;
11      Select  $A' \in \mathbf{A}'$  and augment  $I$  to get  $I'$ ;
12      Generate  $R' \sim \theta^k(I', Q, A', P_{\text{aot}})$ ;
13      if  $A$  is in the final step of  $R$  and  $A'$  is in the final step of  $R'$  and no repetition in  $R$  then
14        Add  $(I, Q, R, R')$  to  $D^k$ ;
15        Add  $(I, Q, A, \mathbf{A}')$  to the set of used samples  $\mathcal{S}$ ;
16      end
17    end
18  end
19  // # Optimization Phase
20  Initialize reference model  $\theta_{\text{ref}}^k = \theta^k$  and keep it frozen;
21  Divide  $D^k = \{(I_i, Q_i, R_i, R'_i)\}_{i=1}^M$  into batches of size  $B$ ;
22  for each batch  $b \subset D^k$  do
23    Compute  $L_{DPO}$  for all samples in batch  $b$ ;
24
25    
$$L_{DPO} = -\frac{1}{B} \sum_{i \in b} \log \sigma \left( \beta \log \frac{\pi_{\theta^k}(R_i|I_i, Q_i)}{\pi_{\theta_{\text{ref}}^k}(R_i|I_i, Q_i)} \right. \\ \left. - \beta \log \frac{\pi_{\theta^k}(R'_i|I_i, Q_i)}{\pi_{\theta_{\text{ref}}^k}(R'_i|I_i, Q_i)} \right)$$

26
27    Update  $\theta^k$  using the accumulated  $L_{DPO}$ ;
28  end
29  // # Evaluation Phase
30  Calculate the average performance  $P^k$  of  $\theta^k$  on three reasoning benchmarks;
31  if  $P^k > P_{\text{best}}$  then
32     $P_{\text{best}} \leftarrow P^k$ ;
33     $\theta^K \leftarrow \theta^k$ ;
34     $K \leftarrow k$ ;
35     $\theta^{k+1} \leftarrow \theta^k$ ;
36     $k \leftarrow k + 1$ ;
37  end
38 else
39   // # Stop iterating when performance saturates
40   break;
41 end
42 return  $\theta^K, K$ ;
```

Prompt: Break down the question into sub-questions

<|begin_of_text|><|start_header_id|>system<|end_header_id|>

You are a helpful, highly intelligent guided assistant. You will do your best to guide humans in choosing the right answer to the question. Note that insufficient information to answer questions is common. The final answer should be one of the options. <|eot_id|><|start_header_id|>user<|end_header_id|>

Given the context, questions and options, please think step-by-step about the preliminary knowledge to answer the question, deconstruct the problem as completely as possible down to necessary sub-questions based on context, questions and options. Then with the aim of helping humans answer the original question, try to answer the sub-questions. The expected answering form is as follows:

Sub-questions:

1. <sub-question 1>
2. <sub-question 2>

...

Sub-answers:

1. <sub-answer 1> or 'Uncertain'
2. <sub-answer 2> or 'Uncertain'

...

Answer: <One of the options> or 'Uncertain'

For a question, assume that you do not have any information about the picture, but try to answer the sub-questions and prioritize whether your general knowledge can answer it, and then consider whether the context can help. If sub-questions can be answered, then answer in as short a sentence as possible. If sub-questions cannot be determined without information in images, please formulate corresponding sub-answer into "Uncertain".

Only use "Uncertain" as an answer if it appears in the sub-answers. All answers are expected as concise as possible.

Here is an attempt:

Context: N/A

Has An Image: yes

[Question][Choices] <|eot_id|><|start_header_id|>assistant<|end_header_id|>

Prompt: Summarize the MLLM output into a rationale.

<|begin_of_text|><|start_header_id|>system<|end_header_id|>

You are a helpful, highly intelligent teacher. You will not only do your best to guide humans to the correct answer, but you will also give the rationales as a reference. <|eot_id|><|start_header_id|>user<|end_header_id|>

Given the context, questions, options, preliminary knowledge, think step by step and answer the questions. Please note that we need not only the answer, but more importantly the rationales of getting the answer. The expected answering form is as follows:

Rationale: <rationale>

Answers: <one of the options>

Please note that the preliminary knowledge given may not always be valid. Please select valid information to form the rationale and choose the relatively correct option as your answer.

Here is an attempt:

Context: N/A

Has An Image: yes

[Question][Choices]

Preliminary knowledge:

[Prior Knowledge] <|eot_id|><|start_header_id|>assistant<|end_header_id|>

Figure 5. The prompts used in DD-Cot for decomposing questions and summarizing MLLM outputs to generate rationale.

Prompt: Extract scene graph

[Question][Choices]

For the provided image and its associated question, generate a scene graph in JSON format that includes the following:

1. Objects that are relevant to answering the question.
2. Object attributes that are relevant to answering the question.
3. Object relationships that are relevant to answering the question.

Scene Graph:

Prompt: Generate rationale based on scene graph information

[Scene Graph]

Use the image and scene graph as context and answer the following question: [Question][Choices]

Please answer the question step-by-step!

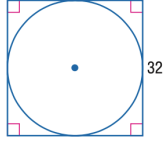
Figure 6. The prompts used in CCot for scene graph extraction and generating rationale based on the scene graph.

Question: Determine the exact circumference of the circle shown.

Choices:

- (A) 16π (B) 32π
(C) 128π (D) 256π

GT: (B) 32π



DD-CoT

[Prior Knowledge] (Sub-questions and Sub-answers)

Question: What is the radius of the circle? Answer: 16

Question: What is the formula for the circumference of a circle? Answer: The formula for the circumference of a circle is $C = 2\pi r$, where C is the circumference and r is the radius.

[Positive Rationale]

To determine the exact circumference of the circle, we need to use the formula for the circumference of a circle, which is $C = 2\pi r$, where C is the circumference and r is the radius. Given that the radius of the circle is 16, we can plug this value into the formula to find the circumference. Therefore, $C = 2\pi(16) = 32\pi$.

Answer: (B) 32π

CCot

[Prior Knowledge] (Scene Graph)

```
{ "objects": [
  { "id": "circle",
    "type": "Circle",
    "center": [16, 16],
    "radius": 16 },
  { "id": "square",
    "type": "Square",
    "corners": [ { "x": 0, "y": 0 }, { "x": 32, "y": 0 },
                 { "x": 32, "y": 32 }, { "x": 0, "y": 32 } ] },
  { "x": 32, "y": 32 }, { "x": 0, "y": 32 } ] },
  "relationships": [
    { "object1": "circle",
      "object2": "square",
      "relationship": "inside" } ] }
```

[Positive Rationale]

To determine the exact circumference of the circle shown in the image, we can use the formula for the circumference of a circle:
 $\text{Circumference} = 2\pi r$
where r is the radius of the circle.

From the image, we can see that the circle is inscribed in a square with a side length of 32 units. The diameter of the circle is equal to the side length of the square, which is 32 units. Therefore, the radius r of the circle is half of the diameter:
 $r = \frac{32}{2} = 16$

Now, we can calculate the circumference: $\text{Circumference} = 2\pi r = 2\pi \times 16 = 32\pi$
So, the exact circumference of the circle shown is: (B) 32π

Naive

[No Prior Knowledge]

[Positive Rationale]

To determine the exact circumference of the circle shown, we can use the relationship between the side length of the square and the radius of the circle.

1. The side length of the square is given as 32 units.
 2. The diameter of the circle is equal to the side length of the square.
 3. Therefore, the radius of the circle is half of the diameter, which is $32/2 = 16$ units.
- The formula for the circumference C of a circle is given by: $C = 2\pi r$, where r is the radius of the circle. Substituting the radius value into the formula: $C = 2\pi \times 16 = 32\pi$
So, the exact circumference of the circle shown is: (B) 32π

[Negative Rationale]

To determine the exact circumference of the circle, we first need to determine its radius.

1. Identify the Side Length of the Square:
 - The square is formed by the sides of the rectangle that is equal to the length of the rectangle's sides.
 - Each side of the square is equal to the height of the rectangle, which is given as 32 units.
2. Find the Radius of the Circle:
 - The diagonal of the square is the diameter of the circle.
 - The diagonal of a square with side length s is given by $s\sqrt{2}$.
 - In this case, the side length s is 32, so the diameter (and hence the radius) is $32\sqrt{2}$.
3. Calculate the Circumference:
 - The circumference C of a circle is given by the formula $C = 2\pi r$, where r is the radius.
 - Using the radius $r = 32\sqrt{2}$:
 $C = 2\pi \times 32\sqrt{2} = 64\sqrt{2}\pi$
 - Simplifying this further, we have:
 $C = 64 \times 1.414\pi = 89.472\pi$

AoT

[Prior Knowledge] (Correct Answer)

The correct answer to the question is "(B) 32π "

[Positive Rationale]

- Step 1, Identify the relationship between the diameter and the circumference of a circle. The formula is $C = \pi d$, where C is the circumference and d is the diameter.
- Step 2, Recognize that the diameter of the circle is equal to the side length of the square, which is given as 32.
- Step 3, Substitute the diameter into the formula: $C = \pi \times 32$.
- Step 4, Simplify the equation: $C = 32\pi$.
- Step 5, Therefore, the exact circumference of the circle is (B) 32π .

[Prior Knowledge] (Incorrect Answer)

The correct answer to the question is "(A) 16π "

[Negative Rationale]

- Step 1, The length of the diagonal of the square is given as 32.
 - Step 2, The diagonal of a square is related to its side length (s) by the equation: $\text{diagonal} = s\sqrt{2}$. Therefore, the side length of the square is $32 / \sqrt{2} = 16$.
 - Step 3, The diameter of the circle is equal to the side length of the square, which is 16.
 - Step 4, The circumference of a circle is given by the formula: $\text{circumference} = \pi \times \text{diameter}$.
 - Step 5, Substituting the diameter of 16 into the formula gives: $\text{circumference} = \pi \times 16 = 16\pi$.
- Final answer: (A) 16π .

Figure 7. Comparison of data generated by different prompts. We remove some symbols, such as \$ and *, for better reading.

Question: What fraction of this is orange?

Choices:

(A) 5/12 (B) 2/11
(C) 7/12 (D) 8/12

GT: (A) 5/12



DD-CoT

[Prior Knowledge] (Sub-questions and Sub-answers)

Question: Is the image a geometric shape? Answer: Yes

Question: Is the shape divided into equal parts? Answer: yes

[Positive Rationale]

Since the shape is a geometric shape and is divided into equal parts, we can assume that it is a circle or a regular polygon. Given that the image is orange, we can infer that the orange area represents a portion of the shape. To determine the fraction of the shape that is orange, we need to analyze the options. Option (A) 5/12 and option (D) 8/12 are both fractions that can be simplified to a common denominator, which is 12. However, option (B) 2/11 cannot be simplified to a common denominator with 12. Therefore, we can eliminate option (B). Between options (A) and (D), we need to determine which one is more likely to be correct. Since the image is not provided, we cannot visually analyze it. However, we can use the fact that the shape is divided into equal parts to make an educated guess. If the shape is a circle, the orange area would likely be a portion of the circle, and the fraction would be less than 1/2. If the shape is a regular polygon, the orange area would likely be a portion of the polygon, and the fraction would be less than 1/2. Therefore, option (A) 5/12 is a more likely answer than option (D) 8/12.

Answer: (A) 5/12

CCoT

[Prior Knowledge] (Scene Graph)

```
{
  "objects": [
    {
      "name": "orange",
      "attributes": { "color": "orange", "shape": "circle", "segments": 12, "fraction": "5/12" } },
    {
      "name": "white",
      "attributes": { "color": "white", "shape": "circle", "segments": 12, "fraction": "7/12" } }
  ],
  "relationships": [
    { "subject": "orange", "object": "orange", "relation": "same_shape" },
    { "subject": "orange", "object": "white", "relation": "same_color" },
    { "subject": "orange", "object": "white", "relation": "same_segments" },
    { "subject": "orange", "object": "white", "relation": "same_fraction" } ]
}
```

[Positive Rationale]

To determine the fraction of the image that is orange, we need to look at the number of segments that are orange compared to the total number of segments in the image.

1. The image shows a circle divided into 12 equal segments.
2. Out of these 12 segments, 5 are shaded orange.

Now, we can calculate the fraction of the image that is orange:

$$\text{Fraction of orange} = \frac{\text{Number of orange segments}}{\text{Total number of segments}} = \frac{5}{12}$$

So, the fraction of the image that is orange is 5/12.

The correct answer is: (A) 5/12

Naive

[No Prior Knowledge]

[Positive Rationale]

Step 1: Identify the total number of parts in the circle.

The circle is divided into 12 equal parts.

Step 2: Determine the number of orange parts.

There are 5 orange parts.

Step 3: Calculate the fraction of the circle that is orange.

The fraction is the number of orange parts divided by the total number of parts.

Fraction = Number of orange parts / Total number of parts

Fraction = 5 / 12

So, the fraction of the circle that is orange is 5/12.

The correct answer is (A) 5/12.

[Negative Rationale]

To determine the fraction of the image that is orange, let's follow these steps:

1. Identify the total number of parts: The image is divided into 12 equal parts.
2. Count the number of orange parts: In the image, there are 8 orange parts.

Now, we can calculate the fraction of the image that is orange:

$$\text{Fraction of orange} = \frac{\text{Number of orange parts}}{\text{Total number of parts}} = \frac{8}{12}$$

Simplifying the fraction:

$$\frac{8}{12} = \frac{2}{3}$$

However, this fraction does not match any of the given choices. It seems there might have been a misunderstanding in the question or the choices provided. Given the choices:

- (A) 5/12 - (B) 2/11 - (C) 7/12 - (D) 8/12

The correct answer based on the calculation is (D) 8/12.

AoT

[Prior Knowledge] (Correct Answer)

The correct answer to the question is " (A) 5/12 "

[Positive Rationale]

Step 1, Observe the given image and determine the number of equal parts the shape is divided into. The shape is divided into 12 equal parts.

Step 2, Identify the number of orange parts. In the image, 5 of these 12 parts are shaded orange.

Step 3, Calculate the fraction of the shape that is orange by dividing the number of orange parts by the total number of parts. So, the fraction is 5/12.

Step 4, Compare this fraction with the given choices. The correct answer is (A) 5/12.

[Prior Knowledge] (Incorrect Answer)

The correct answer to the question is " (B) 2/11 "

[Negative Rationale]

Step 1, Count the number of orange slices: There are 2 orange slices.

Step 2, Count the total number of slices: There are 11 slices in total.

Step 3, Calculate the fraction of the image that is orange: 2/11.

Step 4, Match this fraction to the given choices: The correct answer is (B) 2/11.

Figure 8. Comparison of data generated by different prompts. We remove some symbols, such as \$ and *, for better reading.

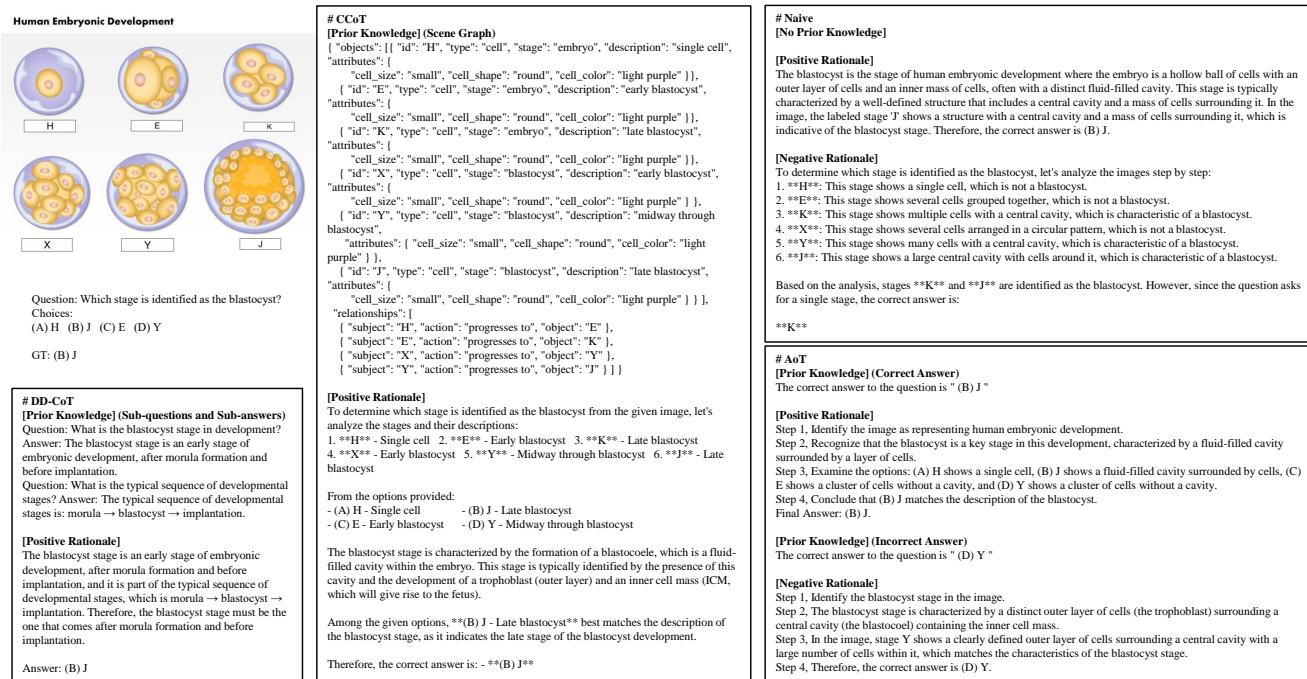


Figure 9. Comparison of data generated by different prompts. We remove some symbols, such as \$ and *, for better reading.

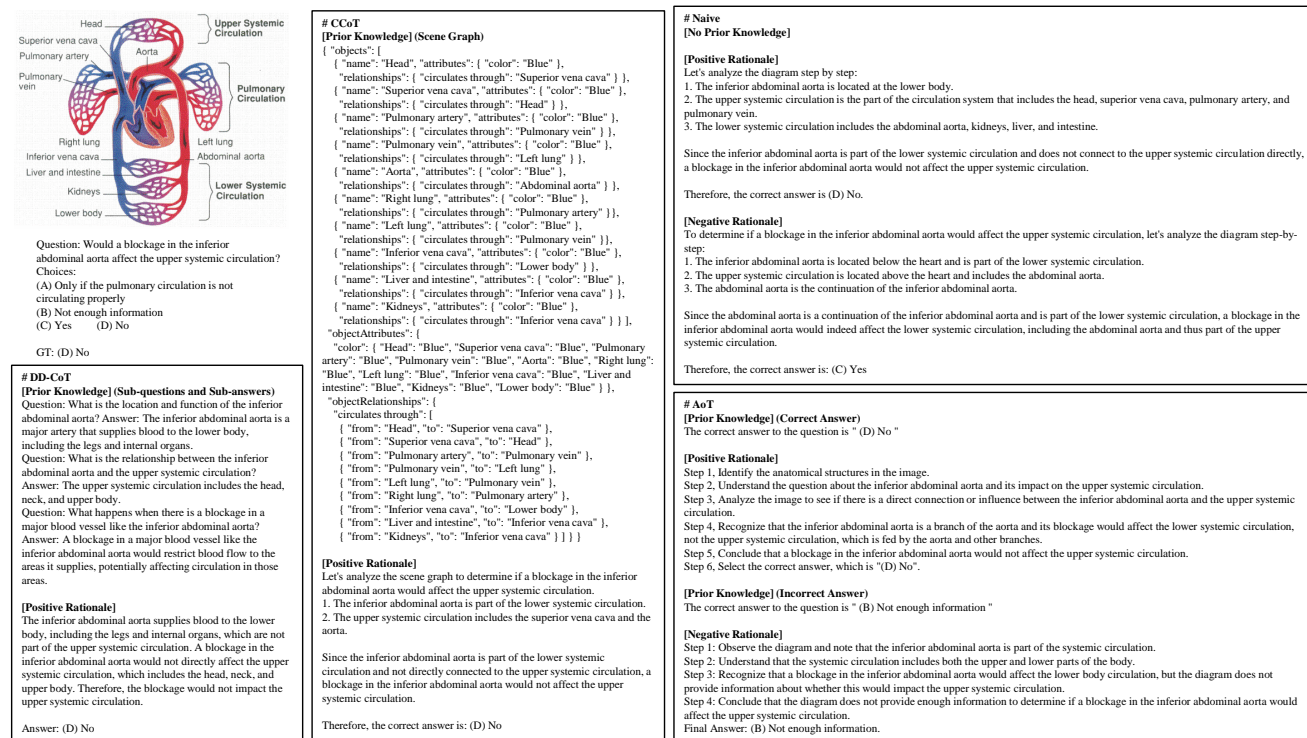


Figure 10. Comparison of data generated by different prompts. We remove some symbols, such as \$ and *, for better reading.

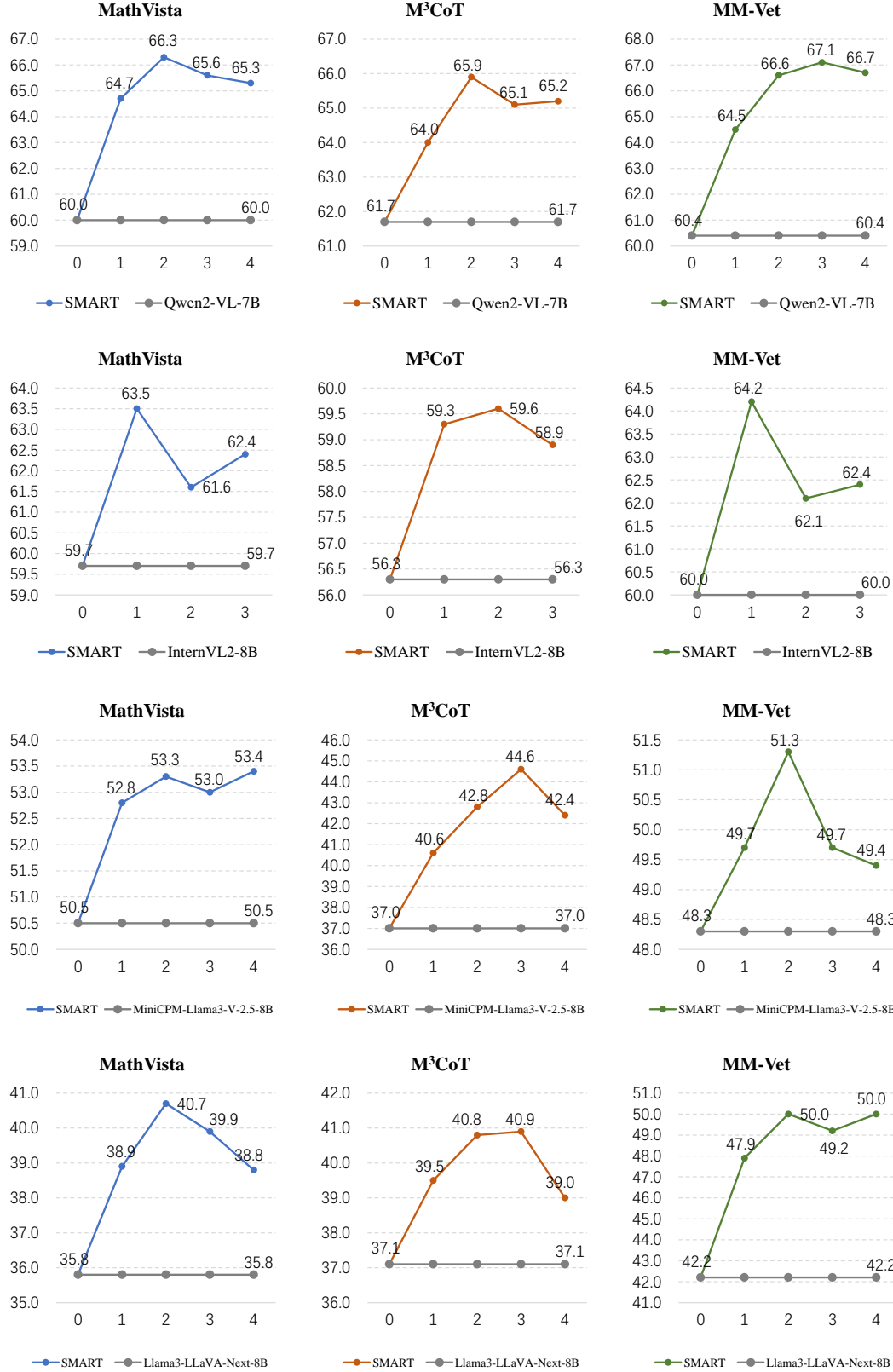


Figure 11. Performance curve of the MLLMs across iterative preference alignment within the SMART framework. The model’s performance quickly improves with more iterations but reaches saturation when it fully exploits its potential, consistent with the observations in [44, 49].

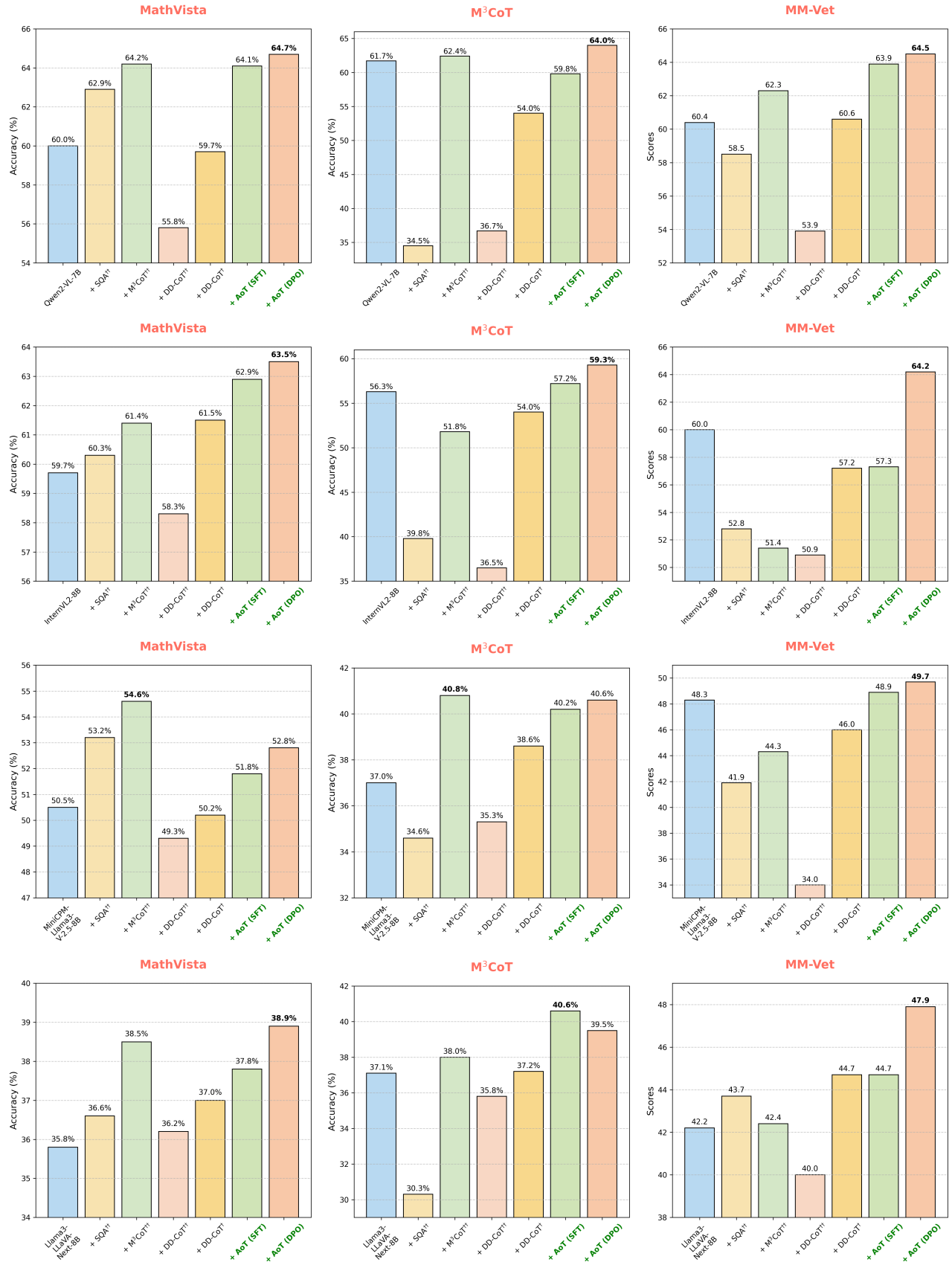


Figure 12. Performance comparison of various models fine-tuned on different reasoning datasets. The results highlight the high quality of AOT data.

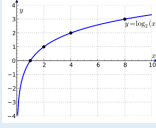
| Prompt | Training Method | MathVista | M ³ CoT | MM-Vet |
|--|-----------------|-----------|--------------------|--------|
| Qwen2-VL-7B | - | 60.0 | 61.7 | 60.4 |
| [Question][Choices] Please answer the question step-by-step! | SFT | 60.6 | 59.4 | 62.3 |
| There is a question about this image, which is '[Question][Choices]'. Please provide concise and direct step-by-step reasoning in the format: 'Step 1, ... Step 2, ...'. Make sure to keep the number of steps as few as possible, and provide the correct answer in the final step. | SFT | 60.5 | 59.6 | 62.8 |
| There is a question about this image, which is '[Question][Choices]'. The correct answer to the question is '[Answer]'. Why? Please provide concise and direct step-by-step reasoning in the format: 'Step 1, ... Step 2, ...'. Make sure to keep the number of steps as few as possible, and provide the correct answer in the final step. | SFT | 64.1 | 59.8 | 63.9 |

Figure 13. Comparison of the performance of different prompts. Incorporating answers into the instructions is quite beneficial.

Question: The derivative of y at $x=6$ is ____ that at $x=8$

Choices:
(A) larger than
(B) equal to
(C) smaller than

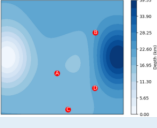
GT: (A) larger than



Question: Which point within the image reaches the deepest depth?

Choices:
(A) Point C (B) Point A
(C) Point D (D) Point B

GT: (D) Point B



Context: In a group of pea plants, some individuals have a tall stem and others have a short stem. In this group, the gene for the stem height trait has two alleles. The allele for a short stem (h) is recessive to the allele for a tall stem (H). This Punnett square shows a cross between two pea plants.

| | | |
|---|----|----|
| | H | H |
| H | HH | HH |
| h | Hh | Hh |

Question: What is the expected ratio of offspring with a tall stem to offspring with a short stem? Choose the most likely ratio.

Choices: (A) 4:0; (B) 1:3; (C) 2:2; (D) 3:1; (E) 0:4

GT: (A) 4:0

Qwen-VL-7B :
To determine the derivative of the function $y = \log_2(x)$ at different points, we need to recall that the derivative of the logarithmic function $y = \log_b(x)$ is given by $\frac{1}{x \ln(b)}$.

For $y = \log_2(x)$, the derivative is:
 $\frac{dy}{dx} = \frac{1}{x \ln(2)}$

Now, let's calculate the derivative at $x = 6$ and $x = 8$:

1. At $x = 6$:
 $\frac{dy}{dx} = \frac{1}{6 \ln(2)}$

2. At $x = 8$:
 $\frac{dy}{dx} = \frac{1}{8 \ln(2)}$

Comparing the two derivatives:
 $\frac{1}{6 \ln(2)} > \frac{1}{8 \ln(2)}$ at $x = 6$ and $\frac{1}{8 \ln(2)}$ at $x = 8$

Since $\frac{1}{6 \ln(2)} > \frac{1}{8 \ln(2)}$, it follows that:
 $\frac{1}{6 \ln(2)} < \frac{1}{8 \ln(2)}$

Therefore, the derivative at $x = 6$ is smaller than the derivative at $x = 8$.

The correct answer is:
(C) smaller than

Qwen-VL-7B + SMART :
The derivative of the function $y = \log_2(x)$ is $\frac{1}{x \ln(2)}$.

At $x = 6$, the derivative is $\frac{1}{6 \ln(2)}$.
At $x = 8$, the derivative is $\frac{1}{8 \ln(2)}$.

Since $6 < 8$, it follows that $\frac{1}{6 \ln(2)} > \frac{1}{8 \ln(2)}$.
Therefore, the derivative of y at $x = 6$ is larger than that at $x = 8$.

The correct answer is:
(A) larger than

Qwen-VL-7B :
To determine which point reaches the deepest depth, we need to look at the color gradient and the contour lines on the map. The color bar on the right side of the image indicates that darker colors represent greater depths.

- Point A is in a light blue area.
- Point B is in a medium blue area.
- Point C is in a light blue area.
- Point D is in a dark blue area.

Since **Point D is in the darkest blue area**, it corresponds to the greatest depth.

Therefore, the point that reaches the deepest depth is: (C) Point D

Please select the correct answer from the ['A'], 'B', 'C', 'D'] options.

The correct answer is:
(C) Point D

Qwen-VL-7B + SMART :
To determine which point reaches the deepest depth, we need to look at the contour map and the color bar on the right side of the image. The color bar indicates the depth in kilometers, with darker shades representing greater depths.

- Point A is located in a light blue region.
- Point B is located in a dark blue region.
- Point C is located in a light blue region.
- Point D is located in a dark blue region.

Since **Point B is in the darkest blue region**, it indicates the deepest depth according to the color bar.

Therefore, the correct answer is:
(D) Point B

Qwen-VL-7B :
To determine the expected ratio of offspring with a tall stem to offspring with a short stem, we need to analyze the Punnett square provided.

The Punnett square shows a cross between two pea plants, both with the genotype Hh (heterozygous for tall stem). The alleles are as follows:
- H: allele for a tall stem (dominant)
- h: allele for a short stem (recessive)

The Punnett square is as follows:

| | | |
|---|----|----|
| | H | H |
| H | HH | HH |
| h | Hh | Hh |

From the Punnett square, we can see the following genotypes for the offspring:
- HH (tall stem) - Hh (tall stem) - Hh (tall stem) - hh (short stem)

The ratio of tall stem to short stem offspring is:
- Tall stem: 3 (HH and Hh)
- Short stem: 1 (hh)

Therefore, the expected ratio of offspring with a tall stem to offspring with a short stem is 3:1.

The correct answer is:
(D) 3:1

Qwen-VL-7B + SMART :
To determine the expected ratio of offspring with a tall stem to offspring with a short stem, we need to analyze the Punnett square provided.

The Punnett square shows a cross between two pea plants, both with the genotype Hh (heterozygous for tall stem). The alleles are as follows:
- H (tall stem, dominant)
- h (short stem, recessive)

The Punnett square is:

| | | |
|---|----|----|
| | H | H |
| H | HH | HH |
| h | Hh | Hh |

From the Punnett square, we can see the following genotypes for the offspring:
- HH (tall stem) - Hh (tall stem) - Hh (tall stem) - hh (tall stem)

All four offspring have the genotype Hh, which results in a tall stem.

Therefore, the expected ratio of offspring with a tall stem to offspring with a short stem is 4:0.

The correct answer is:
(A) 4:0

Figure 14. Additional evaluation results from the Qwen2-VL-7B and SMART models, showcasing SMART's superior reasoning capabilities. To improve readability, we have removed certain symbols, such as \$ and *.

References

- [1] Daechul Ahn, Yura Choi, San Kim, Youngjae Yu, Dongyeop Kang, and Jonghyun Choi. i-srt: Aligning large multimodal models for videos by iterative self-retrospective judgment. *arXiv preprint arXiv:2406.11280*, 2024. 2, 3, 7
- [2] Stanislaw Antol, Aishwarya Agrawal, Jiasen Lu, Margaret Mitchell, Dhruv Batra, C Lawrence Zitnick, and Devi Parikh. Vqa: Visual question answering. In *Proceedings of the IEEE international conference on computer vision*, pages 2425–2433, 2015. 1
- [3] Jinze Bai, Shuai Bai, Shusheng Yang, Shijie Wang, Sinan Tan, Peng Wang, Junyang Lin, Chang Zhou, and Jingren Zhou. Qwen-vl: A frontier large vision-language model with versatile abilities. *CoRR*, abs/2308.12966, 2023. 6
- [4] Silvio Barra, Carmen Bisogni, Maria De Marsico, and Stefano Ricciardi. Visual question answering: Which investigated applications? *Pattern Recognition Letters*, 151:325–331, 2021. 2
- [5] Daniele Calandriello, Daniel Guo, Remi Munos, Mark Rowland, Yunhao Tang, Bernardo Avila Pires, Pierre Harvey Richemond, Charline Le Lan, Michal Valko, Tianqi Liu, et al. Human alignment of large language models through online preference optimisation. *arXiv preprint arXiv:2403.08635*, 2024. 3
- [6] Jun Chen, Deyao Zhu, Xiaoqian Shen, Xiang Li, Zechun Liu, Pengchuan Zhang, Raghuraman Krishnamoorthi, Vikas Chandra, Yunyang Xiong, and Mohamed Elhoseiny. Minigpt-v2: large language model as a unified interface for vision-language multi-task learning. *arXiv preprint arXiv:2310.09478*, 2023. 1
- [7] Keqin Chen, Zhao Zhang, Weili Zeng, Richong Zhang, Feng Zhu, and Rui Zhao. Shikra: Unleashing multimodal llm’s referential dialogue magic. *arXiv preprint arXiv:2306.15195*, 2023. 1
- [8] Qiguang Chen, Libo Qin, Jin Zhang, Zhi Chen, Xiao Xu, and Wanxiang Che. M³cot: A novel benchmark for multi-domain multi-step multi-modal chain-of-thought. *ACL*, 2024. 1, 2, 3, 5, 7
- [9] Zixiang Chen, Yihe Deng, Huizhuo Yuan, Kaixuan Ji, and Quanquan Gu. Self-play fine-tuning converts weak language models to strong language models. *arXiv preprint arXiv:2401.01335*, 2024. 3
- [10] Zhe Chen, Weiyun Wang, Hao Tian, Shenglong Ye, Zhangwei Gao, Erfei Cui, Wenwen Tong, Kongzhi Hu, Jiapeng Luo, Zheng Ma, et al. How far are we to gpt-4v? closing the gap to commercial multimodal models with open-source suites. *arXiv preprint arXiv:2404.16821*, 2024. 1, 5, 6, 2
- [11] Zhe Chen, Jiannan Wu, Wenhai Wang, Weijie Su, Guo Chen, Sen Xing, Muyan Zhong, Qinglong Zhang, Xizhou Zhu, Lewei Lu, et al. Internvl: Scaling up vision foundation models and aligning for generic visual-linguistic tasks. In *Proceedings of the IEEE/CVF Conference on Computer Vision and Pattern Recognition*, pages 24185–24198, 2024. 1
- [12] Wenliang Dai, Junnan Li, Dongxu Li, Anthony Meng Huat Tiong, Junqi Zhao, Weisheng Wang, Boyang Li, Pascale Fung, and Steven Hoi. Instructblip: towards general-purpose vision-language models with instruction tuning. In *Proceedings of the 37th International Conference on Neural Information Processing Systems*, 2024. 3
- [13] Yihe Deng, Pan Lu, Fan Yin, Ziniu Hu, Sheng Shen, James Zou, Kai-Wei Chang, and Wei Wang. Enhancing large vision language models with self-training on image comprehension. *arXiv preprint arXiv:2405.19716*, 2024. 2, 3
- [14] Hanze Dong, Wei Xiong, Bo Pang, Haoxiang Wang, Han Zhao, Yingbo Zhou, Nan Jiang, Doyen Sahoo, Caiming Xiong, and Tong Zhang. Rlhf workflow: From reward modeling to online rlhf. *arXiv preprint arXiv:2405.07863*, 2024. 3
- [15] Abhimanyu Dubey, Abhinav Jauhri, Abhinav Pandey, Abhishek Kadian, Ahmad Al-Dahle, Aiesha Letman, Akhil Mathur, Alan Schelten, Amy Yang, Angela Fan, et al. The llama 3 herd of models. *arXiv preprint arXiv:2407.21783*, 2024. 7, 1
- [16] Chaoyou Fu, Peixian Chen, Yunhang Shen, Yulei Qin, Mengdan Zhang, Xu Lin, Zhenyu Qiu, Wei Lin, Jinrui Yang, Xiwu Zheng, et al. Mme: A comprehensive evaluation benchmark for multimodal large language models. *arXiv:2306.13394*, 2023. 1
- [17] Timin Gao, Peixian Chen, Mengdan Zhang, Chaoyou Fu, Yunhang Shen, Yan Zhang, Shengchuan Zhang, Xiwu Zheng, Xing Sun, Liujuan Cao, et al. Cantor: Inspiring multimodal chain-of-thought of mllm. *ACM MM*, 2024. 1, 2, 3
- [18] Shangmin Guo, Biao Zhang, Tianlin Liu, Tianqi Liu, Misha Khalman, Felipe Linares, Alexandre Rame, Thomas Mesnard, Yao Zhao, Bilal Piot, et al. Direct language model alignment from online ai feedback. *arXiv preprint arXiv:2402.04792*, 2024. 2, 3
- [19] Dan Hendrycks, Collin Burns, Saurav Kadavath, Akul Arora, Steven Basart, Eric Tang, Dawn Song, and Jacob Steinhardt. Measuring mathematical problem solving with the math dataset. *arXiv preprint arXiv:2103.03874*, 2021. 3
- [20] Jack Hessel, Jena D Hwang, Jae Sung Park, Rowan Zellers, Chandra Bhagavatula, Anna Rohrbach, Kate Saenko, and Yejin Choi. The abduction of sherlock holmes: A dataset for visual abductive reasoning. In *European Conference on Computer Vision*, pages 558–575. Springer, 2022. 3
- [21] Jonathan Ho, Ajay Jain, and Pieter Abbeel. Denoising diffusion probabilistic models. *Advances in neural information processing systems*, 33:6840–6851, 2020. 4
- [22] Wenyi Hong, Weihang Wang, Ming Ding, Wenmeng Yu, Qingsong Lv, Yan Wang, Yean Cheng, Shiyu Huang, Junhui Ji, Zhao Xue, et al. Cogvlm2: Visual language models for image and video understanding. *arXiv preprint arXiv:2408.16500*, 2024. 1
- [23] Aniruddha Kembhavi, Mike Salvato, Eric Kolve, Minjoon Seo, Hannaneh Hajishirzi, and Ali Farhadi. A diagram is worth a dozen images. In *Computer Vision–ECCV 2016: 14th European Conference, Amsterdam, The Netherlands, October 11–14, 2016, Proceedings, Part IV 14*, pages 235–251. Springer, 2016. 2
- [24] Aniruddha Kembhavi, Minjoon Seo, Dustin Schwenk, Jonghyun Choi, Ali Farhadi, and Hannaneh Hajishirzi. Are

- you smarter than a sixth grader? textbook question answering for multimodal machine comprehension. In *Proceedings of the IEEE Conference on Computer Vision and Pattern Recognition*, pages 4999–5007, 2017. 2
- [25] Takeshi Kojima, Shixiang Shane Gu, Machel Reid, Yutaka Matsuo, and Yusuke Iwasawa. Large language models are zero-shot reasoners. *NeurIPS*, 2022. 3, 1
- [26] Bohao Li, Yuying Ge, Yixiao Ge, Guangzhi Wang, Rui Wang, Ruimao Zhang, and Ying Shan. Seed-bench: Benchmarking multimodal large language models. In *Proceedings of the IEEE/CVF Conference on Computer Vision and Pattern Recognition*, pages 13299–13308, 2024. 1
- [27] Feng Li, Renrui Zhang, Hao Zhang, Yuanhan Zhang, Bo Li, Wei Li, Zejun Ma, and Chunyuan Li. Llava-next-interleave: Tackling multi-image, video, and 3d in large multimodal models. *arXiv preprint arXiv:2407.07895*, 2024. 3, 5
- [28] Junnan Li, Dongxu Li, Silvio Savarese, and Steven Hoi. Blip-2: Bootstrapping language-image pre-training with frozen image encoders and large language models. In *International conference on machine learning*, pages 19730–19742. PMLR, 2023. 1, 3, 7
- [29] Kaixin Li, Yuchen Tian, Qisheng Hu, Ziyang Luo, Zhiyong Huang, and Jing Ma. Mmcode: Benchmarking multimodal large language models for code generation with visually rich programming problems. In *Findings of the Association for Computational Linguistics: EMNLP 2024*, pages 736–783, 2024. 5
- [30] Ziyi Lin, Chris Liu, Renrui Zhang, Peng Gao, Longtian Qiu, Han Xiao, Han Qiu, Chen Lin, Wenqi Shao, Keqin Chen, Jiaming Han, Siyuan Huang, Yichi Zhang, Xuming He, Hongsheng Li, and Yu Jiao Qiao. Sphinx: The joint mixing of weights, tasks, and visual embeddings for multi-modal large language models. *arXiv:2311.07575*, 2023. 1, 3
- [31] Haotian Liu, Chunyuan Li, Qingyang Wu, and Yong Jae Lee. Visual instruction tuning, 2023. 1
- [32] Haotian Liu, Chunyuan Li, Yuheng Li, and Yong Jae Lee. Improved baselines with visual instruction tuning. In *Proceedings of the IEEE/CVF Conference on Computer Vision and Pattern Recognition*, pages 26296–26306, 2024. 6
- [33] Haotian Liu, Chunyuan Li, Yuheng Li, Bo Li, Yuanhan Zhang, Sheng Shen, and Yong Jae Lee. Llava-next: Improved reasoning, ocr, and world knowledge, 2024. 1, 5, 6, 2
- [34] Haoyu Lu, Wen Liu, Bo Zhang, Bingxuan Wang, Kai Dong, Bo Liu, Jingxiang Sun, Tongzheng Ren, Zhuoshu Li, Yaofeng Sun, et al. Deepseek-vl: towards real-world vision-language understanding. *arXiv preprint arXiv:2403.05525*, 2024. 1
- [35] Pan Lu, Ran Gong, Shibiao Jiang, Liang Qiu, Siyuan Huang, Xiaodan Liang, and Song-chun Zhu. Inter-gps: Interpretable geometry problem solving with formal language and symbolic reasoning. In *Proceedings of the 59th Annual Meeting of the Association for Computational Linguistics and the 11th International Joint Conference on Natural Language Processing (Volume 1: Long Papers)*, pages 6774–6786, 2021. 3
- [36] Pan Lu, Swaroop Mishra, Tanglin Xia, Liang Qiu, Kai-Wei Chang, Song-Chun Zhu, Oyvind Tafjord, Peter Clark, and Ashwin Kalyan. Learn to explain: Multimodal reasoning via thought chains for science question answering. *NeurIPS*, 2022. 1, 2, 7
- [37] Pan Lu, Hritik Bansal, Tony Xia, Jiacheng Liu, Chunyuan Li, Hannaneh Hajishirzi, Hao Cheng, Kai-Wei Chang, Michel Galley, and Jianfeng Gao. Mathvista: Evaluating mathematical reasoning of foundation models in visual contexts. In *International Conference on Learning Representations (ICLR)*, 2024. 1, 5
- [38] Ahmed Masry, Xuan Long Do, Jia Qing Tan, Shafiq Joty, and Enamul Hoque. Chartqa: A benchmark for question answering about charts with visual and logical reasoning. In *Findings of the Association for Computational Linguistics: ACL 2022*, pages 2263–2279, 2022. 3
- [39] Chancharik Mitra, Brandon Huang, Trevor Darrell, and Roei Herzig. Compositional chain-of-thought prompting for large multimodal models. In *CVPR*, 2024. 1, 2, 3, 7
- [40] Debjyoti Mondal, Suraj Modi, Subhadarshi Panda, Rituraj Singh, and Godawari Sudhakar Rao. Kam-cot: Knowledge augmented multimodal chain-of-thoughts reasoning. In *Proceedings of the AAAI Conference on Artificial Intelligence*, pages 18798–18806, 2024. 1, 3
- [41] OpenAI. Gpt-4 technical report. *arXiv:2303.08774*, 2023. 7
- [42] OpenAI. Gpt-4v(ision) system card, 2023. 3, 6
- [43] Long Ouyang, Jeffrey Wu, Xu Jiang, Diogo Almeida, Carroll Wainwright, Pamela Mishkin, Chong Zhang, Sandhini Agarwal, Katarina Slama, Alex Ray, et al. Training language models to follow instructions with human feedback. *Advances in neural information processing systems*, 35:27730–27744, 2022. 3
- [44] Richard Yuanzhe Pang, Weizhe Yuan, Kyunghyun Cho, He He, Sainbayar Sukhbaatar, and Jason Weston. Iterative reasoning preference optimization. *arXiv preprint arXiv:2404.19733*, 2024. 3, 5, 7, 8
- [45] Zhiliang Peng, Wenhui Wang, Li Dong, Yaru Hao, Shaohan Huang, Shuming Ma, and Furu Wei. Kosmos-2: Grounding multimodal large language models to the world. *arXiv preprint arXiv:2306.14824*, 2023. 1
- [46] Colin Raffel, Noam Shazeer, Adam Roberts, Katherine Lee, Sharan Narang, Michael Matena, Yanqi Zhou, Wei Li, and Peter J Liu. Exploring the limits of transfer learning with a unified text-to-text transformer. *Journal of machine learning research*, 21(140):1–67, 2020. 3
- [47] Hao Shao, Shengju Qian, Han Xiao, Guanglu Song, Zhuofan Zong, Letian Wang, Yu Liu, and Hongsheng Li. Visual cot: Unleashing chain-of-thought reasoning in multi-modal language models. *arXiv preprint arXiv:2403.16999*, 2024. 3
- [48] Wenhao Shi, Zhiqiang Hu, Yi Bin, Junhua Liu, Yang Yang, See-Kiong Ng, Lidong Bing, and Roy Ka-Wei Lee. Mathllava: Bootstrapping mathematical reasoning for multimodal large language models. *arXiv preprint arXiv:2406.17294*, 2024. 3, 6
- [49] Wentao Tan, Qiong Cao, Yibing Zhan, Chao Xue, and Changxing Ding. Beyond human data: Aligning multimodal large language models by iterative self-evolution. *arXiv preprint arXiv:2412.15650*, 2024. 2, 3, 5, 7, 8
- [50] Gemini Team, Rohan Anil, Sebastian Borgeaud, Yonghui Wu, Jean-Baptiste Alayrac, Jiahui Yu, Radu Soricut, Johan

- Schalkwyk, Andrew M Dai, Anja Hauth, et al. Gemini: a family of highly capable multimodal models. *arXiv preprint arXiv:2312.11805*, 2023. 6
- [51] Junyang Wang, Yuhang Wang, Guohai Xu, Jing Zhang, Yukai Gu, Haitao Jia, Ming Yan, Ji Zhang, and Jitao Sang. An llm-free multi-dimensional benchmark for mllms hallucination evaluation. *arXiv preprint arXiv:2311.07397*, 2023. 1
- [52] Peng Wang, Shuai Bai, Sinan Tan, Shijie Wang, Zhihao Fan, Jinze Bai, Keqin Chen, Xuejing Liu, Jialin Wang, Wenbin Ge, Yang Fan, Kai Dang, Mengfei Du, Xuancheng Ren, Rui Men, Dayiheng Liu, Chang Zhou, Jingren Zhou, and Junyang Lin. Qwen2-vl: Enhancing vision-language model’s perception of the world at any resolution. *arXiv preprint arXiv:2409.12191*, 2024. 1, 5, 6, 7, 2
- [53] Xiyao Wang, Jiuhai Chen, Zhaoyang Wang, Yuhang Zhou, Yiyang Zhou, Huaxiu Yao, Tianyi Zhou, Tom Goldstein, Parminder Bhatia, Furong Huang, et al. Enhancing visual-language modality alignment in large vision language models via self-improvement. *arXiv preprint arXiv:2405.15973*, 2024. 2
- [54] Yifan Wu, Pengchuan Zhang, Wenhan Xiong, Barlas Oguz, James C Gee, and Yixin Nie. The role of chain-of-thought in complex vision-language reasoning task. *arXiv preprint arXiv:2311.09193*, 2023. 1, 2
- [55] Yuan Yao, Tianyu Yu, Ao Zhang, Chongyi Wang, Junbo Cui, Hongji Zhu, Tianchi Cai, Haoyu Li, Weilin Zhao, Zhihui He, et al. Minicpm-v: A gpt-4v level mllm on your phone. *arXiv preprint arXiv:2408.01800*, 2024. 1, 5, 6, 2
- [56] Qinghao Ye, Haiyang Xu, Jiabo Ye, Ming Yan, Anwen Hu, Haowei Liu, Qi Qian, Ji Zhang, and Fei Huang. mplug-owl2: Revolutionizing multi-modal large language model with modality collaboration. In *Proceedings of the IEEE/CVF Conference on Computer Vision and Pattern Recognition*, pages 13040–13051, 2024. 1
- [57] Alex Young, Bei Chen, Chao Li, Chengen Huang, Ge Zhang, Guanwei Zhang, Heng Li, Jiangcheng Zhu, Jianqun Chen, Jing Chang, et al. Yi: Open foundation models by 01. ai. *arXiv preprint arXiv:2403.04652*, 2024. 1
- [58] Tianyu Yu, Haoye Zhang, Yuan Yao, Yunkai Dang, Da Chen, Xiaoman Lu, Ganqu Cui, Taiwen He, Zhiyuan Liu, Tat-Seng Chua, et al. Rlaif-v: Aligning mllms through open-source ai feedback for super gpt-4v trustworthiness. *arXiv preprint arXiv:2405.17220*, 2024. 3, 5
- [59] Weihao Yu, Zhengyuan Yang, Linjie Li, Jianfeng Wang, Kevin Lin, Zicheng Liu, Xinchao Wang, and Lijuan Wang. Mm-vet: Evaluating large multimodal models for integrated capabilities. *arXiv preprint arXiv:2308.02490*, 2023. 1, 5
- [60] Weizhe Yuan, Richard Yuanzhe Pang, Kyunghyun Cho, Sainbayar Sukhbaatar, Jing Xu, and Jason Weston. Self-rewarding language models. *arXiv preprint arXiv:2401.10020*, 2024. 3
- [61] Eric Zelikman, Yuhuai Wu, Jesse Mu, and Noah Goodman. Star: Bootstrapping reasoning with reasoning. *Advances in Neural Information Processing Systems*, 35:15476–15488, 2022. 3
- [62] Daoan Zhang, Junming Yang, Hanjia Lyu, Zijian Jin, Yuan Yao, Mingkai Chen, and Jiebo Luo. Cocot: Contrastive chain-of-thought prompting for large multimodal models with multiple image inputs. *arXiv preprint arXiv:2401.02582*, 2024. 3
- [63] Zhuosheng Zhang, Aston Zhang, Mu Li, Hai Zhao, George Karypis, and Alex Smola. Multimodal chain-of-thought reasoning in language models. *arXiv preprint arXiv:2302.00923*, 2023. 1, 3
- [64] Ge Zheng, Bin Yang, Jiajin Tang, Hong-Yu Zhou, and Sibe Yang. Ddcot: Duty-distinct chain-of-thought prompting for multimodal reasoning in language models. *NeurIPS*, 2023. 1, 2, 3, 7
- [65] Yiyang Zhou, Zhiyuan Fan, Dongjie Cheng, Sihan Yang, Zhaorun Chen, Chenhang Cui, Xiyao Wang, Yun Li, Linjun Zhang, and Huaxiu Yao. Calibrated self-rewarding vision language models. *arXiv preprint arXiv:2405.14622*, 2024. 3, 5
- [66] Ke Zhu, Liang Zhao, Zheng Ge, and Xiangyu Zhang. Self-supervised visual preference alignment. *ACM MM*, 2024. 2, 3, 4